PPPL-3288, Preprint: February 1998, UC422, 426

Microwave Reflectometry for Magnetically Confined Plasmas

(Accepted for publication in *Review of Scientific Instruments*.)

E. Mazzucato

Princeton University, Princeton Plasma Physics Laboratory, P.O. Box 451, Princeton, New Jersey 08543

This paper is about microwave reflectometry – a radar technique for plasma density measurements using the reflection of electromagnetic waves by a plasma cutoff. Both the theoretical foundations of reflectometry and its practical application to the study of magnetically confined plasmas are reviewed in this paper. In particular, the role of short-scale density fluctuations is discussed at length, both as a unique diagnostic tool for turbulence studies in thermonuclear plasmas, and for the deleterious effects that fluctuations may have on the measurement of the average plasma density with microwave reflectometry.

I. INTRODUCTION

Density measurements play an essential role in the study and operation of magnetically confined plasmas. In existing large devices, such as tokamaks[1], the canonical tools for the measurement of the electron density are laser multichannel interferometry and Thomson scattering[2], two of the most reliable methods in thermonuclear fusion research. Unfortunately, these are also two of the most demanding techniques for plasma accessibility, which ironically is a problem that seems to escalate with the plasma size. Indeed, plasma accessibility will become extremely difficult in a fusion reactor, since it will require penetration not only through the magnetic field coils and the vacuum vessel, as in present experiments, but also through a tritium breeding blanket and a radiation shield. Inevitably, only the simplest diagnostics will survive in such a hostile environment.

Microwave reflectometry, an offspring of radar techniques used in ionospheric studies,[3,4] is a method where the plasma density is inferred from the group delay of electromagnetic waves that are reflected by a plasma cutoff. Since the first application of this method to laboratory plasmas[5,6] and the proposal of employing FM-CW radar techniques in combination with swept millimeter-wave oscillators,[7,8] microwave reflectometry has matured very quickly, and nowadays finds extensive use in tokamak research.[9,67] Its

modest requirement for plasma accessibility and the possibility of conveying microwaves to a remote location make this an ideal method for a fusion reactor.[68-76]

Another area where microwave reflectometry can play a crucial role is in the detection of short-scale turbulence, which appears to be the cause of anomalous transport in high temperature plasmas. As a matter of fact, the first use of reflectometry in tokamaks[77] was not for the measurement of density profiles, but for the detection of density fluctuations. It provided the first evidence for the existence of a small-scale and broad-band turbulence in tokamak plasmas. Reflectometry was then replaced by microwave and laser scattering techniques[78,79] that were capable of providing a more direct measure of wave number spectrum of turbulence. Unfortunately, subsequent measurements[80-82] showed that the scale length of turbulence in tokamaks increases with the plasma size, to the point that scattering methods, with their poor spatial resolution when the turbulence scale length is larger than the wavelength of the probing wave, were no longer capable of separating core from edge phenomena. This led to the reemergence of microwave reflectometry as a diagnostic with good resolution for long wavelength fluctuations.[83-95]

In this paper, we review the application of microwave reflectometry to the measurement of density profiles and to the detection of density fluctuations in magnetically confined plasmas. The paper is organized as follows: Section II is a brief review of the theory of plasma waves that are of interest for reflectometry in magnetized plasmas, i.e., those in the electron cyclotron range of frequencies. Section III is a description of numerical methods for the reconstruction of the electron density distribution from reflectometry measurements. The use of reflectometry for the detection of plasma fluctuations is discussed in Sec. IV. Finally, the reflectometry instrumentation and techniques commonly used in fusion research is reviewed in Sec. V, and future developments are discussed in Sec. VI.

Even though most of the content of this paper is applicable to many types of magnetic configurations, we will often refer to examples taken from tokamak experiments, where reflectometry has found its most extensive use.

II. WAVE THEORY

In a uniform magnetized plasma, a solution of the Maxwell equations in the form of a plane wave $\mathbf{a}\exp(i\mathbf{k}\cdot\mathbf{r}-i\omega t)$ is possible only if the wave vector $\mathbf{k}$ and the frequency ω satisfy a dispersion relation, which in the cold plasma approximation is given by[3,4]

$$D(\mathbf{N},\omega) \equiv \varepsilon_{xx} N_\perp^4 - N_\perp^2[\varepsilon_{xy}^2 + (\varepsilon_{xx} - N_\parallel^2)(\varepsilon_{xx} + \varepsilon_{zz})] + \varepsilon_{zz}[(\varepsilon_{xx} - N_\parallel^2)^2 + \varepsilon_{xy}^2] = 0 \qquad (1)$$

in the system of orthogonal coordinates with basis $(\mathbf{e}_x, \mathbf{e}_y, \mathbf{e}_z)$, where $\mathbf{B} = B\mathbf{e}_z$ is the magnetic field, $\mathbf{N} \equiv \mathbf{k}c/\omega = N_\perp \mathbf{e}_x + N_\parallel \mathbf{e}_z$ is the wave index of refraction, and the only non-zero components of the Hermitian dielectric tensor ε are

$$\begin{aligned} \varepsilon_{xx} &= \varepsilon_{yy} = 1 - \frac{\omega_p^2}{\omega^2 - \omega_c^2} \ , \\ \varepsilon_{xy} &= -\varepsilon_{yx} = \mathrm{i}\frac{\omega_c \omega_p^2}{\omega(\omega^2 - \omega_c^2)} \ , \\ \varepsilon_{zz} &= 1 - \frac{\omega_p^2}{\omega^2} \ , \end{aligned} \qquad (2)$$

where $\omega_p = (4\pi n_e e^2/m_e)^{1/2}$ is the plasma frequency, and $\omega_c = eB/m_e c$ is the electron cyclotron frequency. The solution of Eq. (1) gives two characteristic modes of propagation, the O and the X-mode, with refractive indexes

$$\begin{aligned} N_{\perp O}^2 &= 1 - N_\parallel^2 - X + \frac{XY}{2}\frac{\Delta - Y(1 - N_\parallel^2)}{1 - X - Y^2} \ , \\ N_{\perp X}^2 &= 1 - N_\parallel^2 - X - \frac{XY}{2}\frac{\Delta + Y(1 - N_\parallel^2)}{1 - X - Y^2} \ , \end{aligned} \qquad (3)$$

where $X = \omega_p^2/\omega^2$, $Y = \omega_c/\omega$, and $\Delta = [(1 - N_\parallel^2)^2 Y^2 + 4N_\parallel^2(1 - X)]^{1/2}$. From Eq. (3), we get that one (and only one) value of $N^2 = N_\perp^2 + N_\parallel^2$ is zero when $X = 1$, $X = 1 - Y$, or $X = 1 + Y$. These conditions are referred to in the literature as the O, R, and L cutoff conditions, respectively, and the frequencies where they are satisfied

$$\omega_O = \omega_p \ , \ \omega_R = (\omega_c^2/4 + \omega_p^2)^{1/2} + \omega_c/2 \ , \ \omega_L = (\omega_c^2/4 + \omega_p^2)^{1/2} - \omega_c/2 \ , \qquad (4)$$

are called the cutoff frequencies. From Eq. (4), we get that $\omega_L < \omega_O < \omega_R$ and $\omega_R > \omega_c$. The values of the cutoff frequencies on the equatorial plane of a tokamak plasma are shown in Fig. 1 as a function of the major radius *R* for a plasma with the electron density and temperature profiles of Fig. 2, and a toroidal magnetic field of 5.7 T. These plasma parameters are those envisioned for the International Thermonuclear Experimental Reactor (ITER)[96]. Since at the edge of the plasma column $\omega_p = 0$, and $\omega_O = \omega_L = 0$, both ω_O and ω_L reach a maximum value inside the plasma region, and thus neither of these cutoffs can be used

for probing the full density profile by launching waves from only one side of the torus. On the contrary, ω_R is a decreasing function of the radius whenever $\partial(\omega_p^2 + \omega\omega_c)/\partial R < 0$, so that the full plasma can be probed by launching waves from the low field side of the torus. By using the $\approx R^{-1}$ dependence of the magnetic field in tokamaks, this condition can be written as $\beta < (L_n/R)(\omega/\omega_c)(T/m_e c^2)$, where $L_n = n_e/(\partial n_e/\partial R)$ is the electron density scale length, T is the plasma temperature, and β is the ratio of the plasma to the magnetic pressure.

In a non uniform plasma, where the relative change of plasma parameters is small over an electromagnetic scale length (i.e., the local wavelength and wave period), we may seek solutions of the Maxwell equations in the form

$$\mathbf{a}(\mathbf{r},t)\exp[\mathrm{i}\Phi(\mathbf{r},t)] \tag{5}$$

where is a slowly varying function and $\Phi(\mathbf{r},t)$ is the phase of the electromagnetic field. This is cast in the same form as in the case of a uniform plasma by defining

$$\begin{aligned} &\mathbf{k}(\mathbf{r},t) = \nabla\Phi\,, \\ &\omega(\mathbf{r},t) = -\partial\Phi/\partial t\,, \end{aligned} \tag{6}$$

as the local wave vector and the local frequency, respectively. Then by expanding $\mathbf{a}(\mathbf{r},t)$ in ascending powers of a small dimensionless parameter δ, which is a measure of the fractional change of the background plasma over a wavelength, and assuming Φ of order δ^{-1}, we find[3,4] that the existence of non-trivial solutions to the lowest order equations requires that Eq. (1) be satisfied with $\mathbf{k}$ and ω given by Eq. (6). This equation can be interpreted as providing ω in terms of $\mathbf{k}$, $\mathbf{r}$, and t, i.e., $\omega = \Omega(\mathbf{k},\mathbf{r},t)$. Then using the chain rule on the cross differentiation of Eqs. (6) we obtain

$$\frac{\partial\Omega}{\partial\mathbf{r}} + \frac{\partial\Omega}{\partial\mathbf{k}}\cdot\frac{\partial\mathbf{k}}{\partial\mathbf{r}} + \frac{\partial\mathbf{k}}{\partial t} = 0\,. \tag{7}$$

Finally, by introducing the group velocity $\mathbf{u} = \partial\Omega/\partial\mathbf{k}$, we obtain the ray equations of geometrical optics in Hamiltonian form[3,4,97,98]

$$\begin{aligned} &\frac{\mathrm{d}\mathbf{r}}{\mathrm{d}t} = \mathbf{u} = \frac{\partial\Omega}{\partial\mathbf{k}}\,, \\ &\frac{\mathrm{d}\mathbf{k}}{\mathrm{d}t} = \frac{\partial\mathbf{k}}{\partial t} + \mathbf{u}\cdot\frac{\partial\mathbf{k}}{\partial\mathbf{r}} = -\frac{\partial\Omega}{\partial\mathbf{r}} \\ &\frac{\mathrm{d}\omega}{\mathrm{d}t} = \frac{\partial\Omega}{\partial t}\,. \end{aligned} \tag{8}$$

The phase difference between two points r_1 and r_2 on the same ray is

$$\phi = \int_{r_1}^{r_2} \mathbf{k} \cdot d\mathbf{s} \,, \tag{9}$$

where $d\mathbf{s}$ is the ray path element. In the following, this quantity will be referred to as the phase of geometrical optics. Even though the approximation of geometrical optics is not valid near a wave cutoff, the phase of the reflected wave can be obtained from Eq. (9) together with the condition of reflection at the cutoff point. This can be easily seen by considering the case of a plane stratified plasma in the x-direction, with propagation perpendicular to the magnetic field. Under these conditions, the electromagnetic field is described by a single scalar differential equation

$$\frac{\mathrm{d}^2 E}{\mathrm{d}x^2} + \frac{\omega^2}{c^2} N^2(x) E = 0 \tag{10}$$

with $E \equiv E_z$ for the O-mode, and $E \equiv E_y$ for the X-mode. We consider first the case of a linear wave permittivity $\varepsilon \equiv N^2(x) = 1 - x / x_c$, where the solution of Eq. (10) is given in terms of an Airy integral[3,4,99]

$$\begin{aligned} E(\zeta) &\propto \frac{3}{\pi} \int_0^\infty \cos(x^3/3 - \zeta x)\mathrm{d}x \\ &\approx \frac{3}{\pi^{1/2}\zeta^{1/4}} \cos(2/3\zeta^{3/2} - 1/4\pi) \,, \quad \zeta >> 1 \end{aligned} \tag{11}$$

with $\zeta = (\omega^2 / c^2 x_c)^{1/3}(x_c - x) = [(\omega / c)\, N^2 / 2\, |\mathrm{d}N / \mathrm{d}x|]^{2/3}$. This proves that the solution of geometric optics coincides with the asymptotic approximation of Eq. (11), and thus the phase shift of the reflected wave is

$$\phi = 2\frac{\omega}{c} \int_0^{x_c} N \, dx - \frac{\pi}{2} \tag{12}$$

which, apart from an additive constant, is the same as in Eq. (9). For an arbitrary permittivity, we can still use Eq. (11) inside a narrow layer around the cutoff with a thickness Δ satisfying the condition

$$|\mathrm{d}N^2 / \mathrm{d}x^2|_c \Delta << |\mathrm{d}N / \mathrm{d}x|_c \,, \tag{13}$$

where the subscript indicates the value at . If the value of ζ which corresponds to Δ is much larger than one, we can join the solution of Eq. (11) with that of geometric optics, and thus recover the phase shift of Eq. (12). Since for $\zeta \geq 5$ the accuracy of the asymptotic approximation in Eq. (11) is better than 1%, a condition for the validity of Eq. (12) is

$$|\mathrm{d}N^2/\mathrm{d}x^2|_c << |\mathrm{d}N/\mathrm{d}x|_c^{4/3} k_0^{2/3}/5 \,, \tag{14}$$

where $k_0 = \omega/c$. When $N^2(x)$ has a parabolic profile, for which an exact solution of the wave equation is known, one finds that the inequality (14) can be relaxed and it can be rewritten as[3]

$$|\mathrm{d}N^2/\mathrm{d}x^2|_c < |\mathrm{d}N/\mathrm{d}x|_c^{4/3} \lambda_0^{-2/3} \,, \tag{15}$$

where $\lambda_0 = 2\pi/k_0$. This condition is well satisfied in tokamak plasmas, with the exception of a narrow region near a maximum of the electron density for the O and L-cutoffs, and near the center of plasmas with very high densities for the R-cutoff. At thermonuclear temperatures, the latter densities are not accessible to stable tokamak discharges.

So far, we have neglected the curvature of the magnetic surfaces and considered only the case of a plane stratified plasma. Indeed, this is a good approximation for reflectometry in tokamaks where the probing wave is launched from the low magnetic field side of the equatorial plane perpendicularly to the magnetic surfaces, and with a beam width which is much smaller than the plasma scale.

In the case of the X-mode, we have also neglected the presence of the upper-hybrid resonance layer ($X = 1 - Y^2$) behind the R-cutoff (Fig. 1). The case of wave propagation with back-to-back linear and singular turning points is described in Ref. 4 where it is shown that the wave can tunnel through the evanescent layer with a power transmission $T = \exp(-\pi k_0 \delta/2)$, where δ is the thickness of the layer. Since in tokamaks $k_0\delta >> 1$, with the exception in a small region near the plasma edge, the upper-hybrid resonance is practically inaccessible to the probing wave.

By assuming a magnetic field with a constant direction we have also neglected the shear of the magnetic field lines, that is not necessarily justified for a tokamak plasma. Indeed, for wave propagation perpendicular to the magnetic field $\mathbf{B} = B_y(x)\mathbf{e}_y + B_z(x)\mathbf{e}_z$, the electromagnetic field is described by two coupled differential equations[4,100,101]

$$\begin{aligned} \frac{\mathrm{d}^2 E_\parallel}{\mathrm{d}x^2} + (k_0^2 N_O^2 - \phi^2) E_\parallel &= 2\phi \frac{\mathrm{d}E_\perp}{\mathrm{d}x} + \frac{\mathrm{d}\phi}{\mathrm{d}x} E_\perp \\ \frac{\mathrm{d}^2 E_\perp}{\mathrm{d}x^2} + (k_0^2 N_X^2 - \phi^2) E_\perp &= -2\phi \frac{\mathrm{d}E_\parallel}{\mathrm{d}x} - \frac{\mathrm{d}\phi}{\mathrm{d}x} E_\parallel \end{aligned} \tag{16}$$

where $E_\parallel$ and $E_\perp$ are the electric field components that are respectively parallel and perpendicular to **B**, $\phi = \mathrm{d}\theta/\mathrm{d}x$, and θ is the angle between **B** and $\mathbf{e}_z$. In a typical tokamak discharge, θ is zero on the mag-

netic axis and reaches a maximum value of 0.1-0.3 rad near the plasma boundary, making $k_0^2 >> \phi^2$. From the structure of these equations, it is clear that a substantial coupling between the two modes of propagation is possible only if $N_O \approx N_X$. Thus, deep inside the plasma column, where $N_O \neq N_X$, the coupling is very weak and the wave polarization rotates with the magnetic field. On the contrary, near the plasma edge where the electron density is low and $N_O \approx N_X$, mode coupling is possible and the wave polarization does not follow the magnetic field since it propagates as in vacuum. Since at the edge of a tokamak discharge $\phi \approx 0$, we conclude that mode coupling is not important for reflectometry in tokamaks.

Finally, to avoid total absorption, the probing wave must not cross regions of plasma where its frequency is equal to one of the first harmonics of the electron cyclotron frequency. However, this is not always sufficient because of kinetic effects on the cyclotron resonance condition[102-106]

$$\gamma - n\,\omega_c / \omega - N_\parallel\, w_\parallel = 0 \ , \qquad (17)$$

where $\mathbf{p}$ is the electron momentum, $p = |\mathbf{p}|$, $p_\parallel = \mathbf{p}\cdot\mathbf{B}/B$, $w = p/mc$, $w_\parallel = p_\parallel / mc$, $\gamma = (1+w^2)^{1/2}$, and n is the harmonic number. Indeed, in high temperature plasmas the cyclotron resonance is broadened and down-shifted by the relativistic change of the electron mass even for quasi-perpendicular propagation ($N_\parallel \approx 0$). For a description of the kinetic theory of linear wave absorption we refer to Refs. 102-106. Here it is sufficient to mention that the introduction of kinetic effects produces an anti-Hermitian component of the dielectric tensor, with the result that the solution of the dispersion relation becomes a complex wave vector $\mathbf{k} = \mathbf{k}_r + i\mathbf{k}_i$. For the case of interest in reflectometry where $|\mathbf{k}_r| >> |\mathbf{k}_i|$, it is possible to reformulate the theory of geometric optics with new ray equations that are expressed in terms of the real part of the dispersion relation and $\mathbf{k}_r$,[98,102] and with a wave damping that is given by the integral along the ray trajectory $\int \mathbf{k}_i \cdot d\mathbf{s}$. Of the three types of waves used in reflectometry, R-waves are the most sensitive to relativistic effects.[107] This is illustrated in Figs. 3 and 4 for the plasma conditions of Fig. 2, where use is made of a relativistic dielectric tensor that includes the contribution of the first three cyclotron harmonics.[108] Figure 3 shows the ray trajectory of a wave with a frequency of 185 GHz, launched with the X-mode perpendicularly to the magnetic field. Also shown in Fig. 3 is the cutoff surface $\omega = \omega_R$ of the cold plasma approximation, and that given by the relativistic theory. For the same plasma conditions of Fig. 2 and the launching geometry of Fig. 3, Fig. 4 shows the fraction of power that is absorbed in the round-trip of an R-wave as a function of its frequency. These results illustrate the importance of the relativistic correc-

tion to the absorption of R-waves in reflectometry of hot plasmas, as in the case of Fig. 4 where the high field side of the density profile becomes inaccessible to the probing wave. On the contrary, the other two types of waves (L and O) used in reflectometry are less sensitive to relativistic effects. For the same plasma conditions of Fig. 2, we find that wave absorption is negligible for both O and L waves, even though there is still a substantial relativistic correction to the position of the O-cutoff near the plasma center. Finally, in the range of electron temperatures of existing tokamaks (< 10 keV), the wave absorption is negligible for reflectometry, but the propagation of R-waves may still be affected by relativistic effects. Fortunately, this phenomenon can be reproduced using the cold dielectric tensor (Eq. (2)) together with a simple change of the electron mass [109]

$$m = m_e(1+5/\mu)^{1/2} \ , \qquad (18)$$

where $\mu = m_e c^2 / T_e$. For the X-mode, which is the only case of interest, the validity of this equation requires $\mu(1-\omega_c/\omega) >> 1$, a condition that is well satisfied in plasmas of existing large tokamaks.

III. DENSITY MEASUREMENTS

In microwave reflectometry, the basic information for inferring the plasma density is the phase delay of the reflected wave. In general, the launching direction is such that the wave trajectory remains quasi-parallel to the plasma density gradient, and thus quasi-perpendicular to the magnetic field (Fig. 3). These conditions are not strictly necessary, but they greatly simplify the collection and the analysis of data. From Eq. (9), the phase delay is given by

$$\phi(\omega) = 2\frac{\omega}{c}\int_{x_0}^{x_c(\omega)} N(\omega,x)\, dx + \phi_0(\omega) \ , \qquad (19)$$

where x_0 and $x_c (> x_0)$ are respectively the coordinates of the plasma boundary and the cutoff layer, and $\phi_0(\omega)$ is the phase delay that the wave suffers outside of the plasma. The latter can be either calculated or measured independently. To simplify the notations, in the following we will assume that $\phi_0(\omega)$ has been subtracted from the measured phase, and we will denote with $\phi(\omega)$ the first term on the right hand side of Eq. (19).

The electron density profile can be inferred from the frequency dependence of $\phi(\omega)$, that can be measured by sweeping the frequency of the probing wave. On the other hand, since the phase of a wave can

be measured only relative to the unknown phase of a reference signal, the direct output of a reflectometer system is $d\phi(\omega)/d\omega$, rather than $\phi(\omega)$. Indeed, this is a quantity with a clear physical meaning since, by recalling the first of Eqs. (8) and using the identity $N(\omega, x_c) = 0$, we get

$$\frac{d\phi(\omega)}{d\omega} = 2\int_{x_0}^{x_c(\omega)} \frac{dx}{u} , \tag{20}$$

which is the round-trip group delay of the probing wave. For propagation perpendicular to the magnetic field, the cold plasma approximation gives

$$\begin{aligned} u_O &= c\,N_O , \\ u_X &= c\,N_X \frac{(1-X-Y^2)^2}{(1-X-Y^2)^2 + XY^2} \end{aligned} \tag{21}$$

for the group velocity of the O and the X-mode, respectively. In ionospheric studies, because of the large distance between the launcher and the reflecting layer, the group delay is obtained directly from the time of flight of short pulses.[3,4] In laboratory plasmas, the group delay is instead obtained from phase measurements. Nevertheless, recent technological advances are beginning to make the ionospheric approach feasible in laboratory plasmas as well.[33,34,36,46,49,62,69,74,]

When $x_c(\omega)$ is a monotonic function of frequency, the electron density profile can be obtained by inverting Eq. (20). For the O-mode in the cold plasma approximation, this can be done analytically since v_O is only a function of ω and of the local cutoff frequency $\omega_O = \omega_p$. By using the latter as the independent variable, it is easy to show that Eq. (20) can be converted into an Abel integral equation[4] whose solution is

$$x_c(\omega_p) = x_0 + \frac{c}{\pi}\int_0^{\omega_p} \frac{d\phi(\omega)/d\omega}{(\omega_p^2 - \omega^2)^{1/2}}\, d\omega \ . \tag{22}$$

In practice, since it is not possible to measure the group delay from $\omega = 0$, the value of $d\phi(\omega)/d\omega$ up to the lowest employed frequency ω_0 must be obtained from other density measurements, or, in the absence of data, by assuming a shape for the density edge profile. For the X-mode, and in those cases where relativistic corrections must be taken into account, the inversion of Eq. (20) cannot be performed analytically since the group velocity is an explicit function of position. In these cases, the inversion of Eq. (20)

can be calculated numerically with the following procedure. Let $x_0 = 0$ be the known cutoff position corresponding to the lowest frequency ω_0, ω_1, $\omega_2 .... \omega_n$ be the frequencies where the group delay is measured, and define

$$\tau_i = (d\phi(\omega)/d\omega)_{\omega=\omega_i},$$
$$\varphi_i = \sum_{j=1}^{i} \tau_j(\omega_j - \omega_{j-1}) . \qquad (23)$$

Again, to simplify the notations, we assume that the contribution of the edge region $x < x_0$ to the wave group delay has been subtracted from the measured value of $d\phi(\omega)/d\omega$. Let x_i be the cutoff position of the frequency ω_i, and define $A_{i,j} = \omega_i(N_{i,j} + N_{i,j-1})/2c$, where $1 \le j \le i$, $N_{i,j}$ is the refractive index for $\omega = \omega_i$ and $x = x_j$, and $N_{i,i} = 0$ .by definition. Then Eq. (19) becomes for all values of *i*

$$\varphi_i = \sum_{j=1}^{i} A_{i,j}(x_j - x_{j-1}) , \qquad (24)$$

which in matrix notation can be written as

$$\begin{bmatrix} \phi_1 \\ \phi_2 \\ \phi_3 \\ \cdot \\ \phi_n \end{bmatrix} = \begin{bmatrix} A_{1,1} & 0 & 0 & \cdot \\ A_{2,1} - A_{2,2} & A_{2,2} & 0 & \cdot \\ A_{3,1} - A_{3,2} & A_{3,2} - A_{3,3} & A_{3,3} & \cdot \\ \cdot & \cdot & \cdot & \cdot \\ A_{n,1} - A_{n,2} & A_{n,2} - A_{n,3} & A_{n,3} - A_{n,4} & \cdot \end{bmatrix} \begin{bmatrix} x_1 \\ x_2 \\ x_3 \\ \cdot \\ x_n \end{bmatrix} , \qquad (25)$$

or more concisely

$$\phi = \mathbf{M} \cdot \mathbf{x} . \qquad (26)$$

For the O-mode in the cold plasma approximation, the matrix $\mathbf{M}$ is not an explicit function of x_i, and thus the vector $\mathbf{x}$ can be easily obtained by inverting Eq. (26)

$$\mathbf{x} = \mathbf{M}^{-1} \cdot \phi . \qquad (27)$$

In general, from Eq. (25) we get

$$
\begin{aligned}
&x_1 = \phi_1 / A_{1,1}\,,\\
&x_2 = [x_1(A_{2,2} - A_{2,1}) + \phi_2] / A_{2,2}\,,\\
&x_3 = [x_1(A_{3,2} - A_{3,1}) + x_2(A_{3,3} - A_{3,2}) + \phi_3] / A_{3,3}\,, \qquad ,\\
&\cdots\cdots\cdots\cdots\cdots\cdots\cdots\\
&x_n = [x_1(A_{n,2} - A_{n,1}) + x_2(A_{n,3} - A_{n,2}) \;\cdot\;\cdot\, x_{n-1}(A_{n,n} - A_{n,n-1}) + \phi_n) / A_{n,n}
\end{aligned}
\qquad (28)
$$

that, since x_i is given in terms of x_j with $j < i$, represents the solution of our problem for any type of wave polarization. Once the values of x_i have been determined, the electron density is easily obtained from the known dependence of the cutoff frequencies on plasma parameters. The precision then depends on the accuracy with which the group delays τ_i are measured. As it will be described in Section V, in most reflectometer schemes the received signal is downshifted at a lower frequency ω_s, and the group delay is obtained from phase measurements. These may be considered equivalent to the measurement of the time t at which the waveform crosses the zero axis. In the presence of noise with a large signal-to-noise power ratio (S/N), the rms error is then given by[110] $\delta t = 1/\omega_s(2S/N)^{1/2}$, so that the uncertainty in the position of the cutoff is

$$
\delta x \approx \frac{c}{2\omega_s(2S/N)^{1/2}}\,. \qquad (29)
$$

This equation shows the importance of operating at large frequencies,[71] which allows a better statistical averaging of the results as well.

As we shall see in the next Section, a much more serious deterioration in the accuracy of density measurements is caused by the large amplitude and phase modulations which are induced on the measured signals by 2D density fluctuations.

IV. FLUCTUATION MEASUREMENTS

As mentioned in the Introduction, microwave reflectometry is also a tool for the detection of plasma fluctuations, even though the extraction of quantitative information from the measured signals is often very difficult. This Section is a review of this subject.

In the presence of density fluctuations, the interpretation of reflectometry data is relatively simple when the plasma permittivity varies only along the direction of propagation of the probing wave. In the

plane stratified geometry of Sec. II, this can be easily seen by taking a wave permittivity in the form $\varepsilon = \varepsilon_0(x) + \tilde{\varepsilon}(x)$, and by assuming that the probing wave is launched along the *x*-axis. Then by solving the wave equation with the method of successive approximations, the first order term (Born approximation) outside of the plasma region ($x < 0$) is, apart from a constant phase,[111-115]

$$E_1 = 2k_0 \exp(ik_0 x) \int_0^\infty \tilde{\varepsilon}(r) A^2(r) dr \ , \qquad (30)$$

where $A(x)$ is a zero order solution of the wave equation with $A(x) \to 0$ for $x \to \infty$, and $A(x) \to \cos(k_0 x + \varphi)$ for $x \to 0$. As discussed in Sec. II, both $A(x)$ and the zero order field E_0 are given by the Airy function Ai when $\varepsilon_0(x)$ is a linear function. If $|E_1| << |E_0|$, Eq. (30) is a good approximation of the total scattered field, and by casting the backward wave in the form $\exp(ik_0 x) + i\phi)$, it gives the contribution of fluctuations to the phase of the reflected wave

$$\tilde{\phi} = 2k_0 \int_0^\infty \tilde{\varepsilon}(x) A^2(x) dx \ . \qquad (31)$$

On the other hand, by expanding $\sqrt{\varepsilon}$ to the first order in $\tilde{\varepsilon}$, from Eq. (12), we obtain

$$\tilde{\phi} = k_0 \int_0^{x_c} \frac{\tilde{\varepsilon}}{\sqrt{\varepsilon_0}} \, dx \ . \qquad (32)$$

Away from the cutoff point, where $A(x) \approx \varepsilon_0^{-1/4} \cos(k_0 \int_0^x \sqrt{\varepsilon_0(r)} dr - \pi / 4)$ (WKBJ approximation[3,4]), the coefficient of $\tilde{\varepsilon}$ in the integrand of Eq. (32) is the average over a distance $\Delta x = \pi / k_0 \varepsilon_0^{1/2}$ of a similar coefficient in Eq. (31). This is not true near the cutoff where $\varepsilon_0^{-1/2} \to \infty$ and $A^2 \propto Ai^2(\zeta)$, with $\zeta \equiv (\omega^2 / c^2 L_\varepsilon)^{1/3} (x_c - x)$ and $L_\varepsilon^{-1} = (d\varepsilon_0 / dx)_{x = x_c}$. Since the WKBJ approximation is valid up to the last lobe of $A^2(\zeta)$, which near $\zeta \approx 0$ has a width $\Delta\zeta \approx 3$ (i.e., $\Delta x \approx 3(k_0 L_\varepsilon)^{1/3} / k_0$), we conclude that Eq. (32) represents a good approximation of the wave phase when fluctuations are in the range of wave numbers $|k_x| < k_G \equiv \pi / \Delta x \approx k_0 / (k_0 L_\varepsilon)^{1/3}$, and thus the scattered field is strongly weighted by the region near the cutoff. On the contrary, when $|k_x| >> k_G$, the scattered field originates from fluctuations located away from the cutoff where the spatial variation of $A^2(x)$ matches that of the density perturbation (Bragg resonance condition).[112-116] Clearly, only the case with $|k_x| < k_G$ is of interest for the localized detection of fluctuations. In this case, by using the approximation $\varepsilon_0(x) \approx (x_c - x) / L_\varepsilon$, that is valid near the cutoff, from Eq. (32) we obtain the relationship[91]

$$\Gamma_\phi(k_x) = 2\pi \frac{k_0^2 L_\varepsilon}{|k_x|}[C^2(w) + S^2(w)]\Gamma_\varepsilon(k_x) \qquad (33)$$

between the power spectra of the permittivity ($\Gamma_\varepsilon(k_x)$) and that of the phase ($\Gamma_\phi(k_x)$), which are defined as the Fourier transforms of the autocorrelation of $\tilde{\varepsilon}$ and $\tilde{\phi}$ (considered as a function of x_c), respectively. The functions $C(w)$ and $S(w)$ in Eq. (33) are the Fresnel integrals[99] with $w = (2|k_x|L_\varepsilon / \pi)^{1/2}$. For the case of interest in tokamaks where $w >> 1$, $C(w) \approx S(w) \approx 1/2$, while for $w << 1$, $C(w) \approx w$ and $S(w) \approx 0$. By using the known dependence of $\tilde{\varepsilon}$ on the density fluctuation $\tilde{n}_e / n_e$, from Eq. (33) we obtain[60]

$$\Gamma_\phi(k_x) = 2\pi M \frac{k_0^2 L_\varepsilon}{|k_x|}[C^2(w) + S^2(w)]\Gamma_n(k_x) \,, \qquad (34)$$

where is the power spectrum of $\tilde{n}_e / n_e$, and M is the value of $(n_e \partial\varepsilon / \partial n_e)^2$ near the cutoff. For wave propagation perpendicular to the magnetic field, M=1 for the O-mode, and M=4 for the X-mode. In conclusion, one dimensional (1D) fluctuations with produce a phase modulation of the probing wave, with a magnitude which is given by geometric optics. Equation (34) can then be used for inferring the spectrum of density fluctuations from the spectrum of the measured phase.

The interpretation of reflectometry becomes considerably more complicated in the case of multidimensional fluctuations, where the plasma permittivity varies perpendicular to the direction of propagation of the probing wave. In this case, even for fluctuations with a wavelength sufficiently long to make geometric optics applicable, the measured backward field cannot be described as a specular reflection of the probing wave, as in the case of 1D fluctuations, and more important, its properties can differ drastically from those of plasma fluctuations. This can be easily seen by taking the wave permittivity $\varepsilon = \varepsilon_0(x) + \tilde{\varepsilon}(x,y)$ in the same system of coordinates of the previous paragraph, and assuming that near the cutoff the reflected wave can be cast in the form $\exp(i\tilde{\phi}(y))$, with $\tilde{\phi}(y)$ given by Eq. (12). In a random medium, as in the case of a tokamak where the plasma density is perturbed by a short-scale turbulence, the phase of the probing wave is the cumulative result of many random contributions, so that it is reasonable to assume that $\tilde{\phi}$ is a normal random variable with mean $<\tilde{\phi}>=0$, variance $\sigma_\phi^2 \equiv <\tilde{\phi}^2>$ and normalized autocorrelation $\gamma_\phi(\xi) \equiv <\tilde{\phi}_1(y)\tilde{\phi}_2(y+\xi)> / \sigma_\phi^2$. From this, we get that the first moment of the wave electric field, which can be interpreted as the amplitude of a coherent specular reflection, is $<E>=\exp(-\sigma_\phi^2/2)$, and thus it is a decreasing function of σ_ϕ. For the second moment we get $<E_1 E_2^*>=\exp[-\sigma_\phi^2(1-\gamma_\phi)]$, which proves

that the signal correlation length is also a decreasing functions of σ_ϕ. In particular, for $\sigma_\phi >> 1$, taking $\gamma_\phi(\xi) = \exp[-(\xi/\Delta)^2]$ and expanding to the second order in ξ, we obtain $< E_1 E_2^* > \approx \exp[-(\sigma_\phi \xi/\Delta)^2]$. Thus in the presence of 2D density fluctuations, the spectrum of reflected waves can become broader than the spectrum of $\tilde{\phi}$, and consequently broader than the spectrum of plasma fluctuations. Under these conditions, it becomes very difficult to infer the properties of the latter from reflectometry measurements. The problem becomes even more complicated when the approximation of geometric optics is no longer valid, making microwave reflectometry a useless technique for fluctuations studies.

Based in part on these arguments, a model of reflectometry has been proposed[91,94] where the field of scattered waves arises from a phase modulation of the incoming wave, with a magnitude that can be obtained from 1D geometric optics neglecting the effects of fluctuations on ray trajectories. To an observer, the reflected field appears to originate at a virtual location $x \approx x_G = \int_0^{x_c} dx/u$, corresponding to the average round-trip delay. After reflection, the electromagnetic field separates into a wave propagating along the direction of specular reflection, and into a group of scattered waves propagating in different directions. The amplitude of the former decreases quickly to an insignificant level ($\approx \exp(-\sigma_\phi^2/2)$) as the variance σ_ϕ^2 of the phase modulation becomes larger than one. The spectral width of scattered waves also increases with the amplitude of fluctuation and becomes a factor of σ_ϕ larger than the spectral width of $\tilde{\phi}$. Thus, if Δk_y is the width of fluctuations in the *y*-direction and $\sigma_\phi \Delta k_y << k_0$, the scattered waves are spread over the range of wave numbers $\delta k_x \approx \sigma_\phi^2 \Delta k_y^2 / 2k_0$, so that an observer at a distance from the plane $x = x_G$ which is larger than the *diffraction distance* $D = \delta k_x^{-1}$ will sample a complicated interference pattern, with large amplitude variations and random phases. This suggests[93] that the amplitude $\rho \equiv |s|$ of the received signal s should follow the distribution derived by Rice[117,118] for a signal containing a sinusoidal component, and a Gaussian noise having independent normal random variables for its real and imaginary parts. For such a signal, the amplitude ρ has the distribution

$$P(\rho) = \frac{\rho}{\sigma^2} \mathrm{e}^{-(\rho^2 + s_0)/2\sigma^2} I_0\left(\frac{\rho s_0}{\sigma^2}\right), \qquad (35)$$

where I_0 is the modified Bessel function of order zero,[99] σ^2 is the variance of both the real and the imaginary parts of the Gaussian noise, and s_0 is the amplitude of the sinusoidal component. In our case,

assuming that the launched wave has a unit amplitude, we get . Figure 5 illustrates two examples taken from a TFTR experiment,[119] where the amplitude distribution of the measured signal in the far field region () is compared with the Rice distribution that best fits the experimental data. From this we get a value for s_0, that together with the equation $s_0 = \exp(-\sigma_\phi^2/2)$, gives =0.4 and σ_ϕ=0.75 rad, respectively. Even though these values for σ_ϕ depend on the assumed distribution of $\tilde{\phi}$ near the cutoff, the excellent agreement of the experimental signal distribution with Eq. (35) is a strong indication that the measured scattered waves resemble a Gaussian noise. Hence the conclusion that the spectrum of plasma fluctuations cannot be inferred from phase measurements, if these are made where $|x - x_G| \geq D$.

A crucial assumption in the proposed model of reflectometry is that the measured reflected wave appears to originate from a virtual location behind the reflecting layer, and to arise from a phase modulation of the probing wave, with an amplitude given by 1D geometric optics. Numerical solutions of the wave equation in the presence of 2D fluctuations indicate that this is indeed a valid approximation when the amplitude of fluctuations is not too large.[120] An example is given in Fig. 6, which shows the amplitude ($|E|$) of the backward field, and the fluctuating component ($\tilde{\phi}$) of its phase at the cutoff virtual location. These results refer to the case of a probing wave with a frequency of 75 GHz and the O-mode, in a TFTR-like plasma with density fluctuations having the power spectrum , with =1 cm^{-1}, Δk_y=0.5 cm^{-1}, and the volume average $\sigma_n \equiv < \tilde{n}_e^2 / n_e^2 >^{1/2}$=5x10^{-3}. The results in Fig. 6 were obtained by propagating backwards in vacuum the calculated spectrum of reflected waves. They show clearly that, as assumed in the model, the backward field is well approximated by at the cutoff virtual location, with $\tilde{\phi}$ given by 1D geometric optics. On the contrary, at locations where $|x - x_G| \geq D$, as near the plasma boundary (Fig. 7), the calculated backward field is dominated by large amplitude variations and random phases.

This model of reflectometry must fail for large fluctuations. Indeed, since each spectral component of the backward field carries information from a region near its reflecting point, the breakdown of the model must occur when the reflecting points are distributed over a distance Δx_c which is comparable to the wavelength of fluctuations, i.e., when $\Delta x_c \Delta k_x > 1$. Since $\Delta x_c / L_\varepsilon \approx \sigma_\phi^2 \Delta k_y^2 / k_0^2$, we conclude that this condition requires

$$\sigma_\phi^2 < \frac{k_0^2}{L_\varepsilon \Delta k_x \Delta k_y^2} \ . \qquad (36)$$

For fluctuations with a Gaussian spectrum, as those used in the numerical simulation, Eq. (34) gives $\sigma_\phi^2 = \pi^{3/2} M (k_0^2 L_\varepsilon / \Delta k_r)\, \sigma_n^2$, which allows Eq. (36) to be cast in the form

$$\sigma_n^2 < \frac{1}{\pi^{3/2} M L_\varepsilon^2 \Delta k_y^2} \ . \qquad (37)$$

For the case of Fig. 6, where L_ε=50 cm, this gives $\sigma_n \approx 0.02$, in good agreement with the numerical results.[120] Finally, another condition for the use of geometric optics, that also applies to the case of 1D fluctuations, is the absence of local inversions in the plasma permittivity along the initial direction of the probing wave, which for the geometry considered so far requires

$$\sigma_n < \frac{1}{\Delta k_x L_\varepsilon} \ . \qquad (38)$$

A crucial parameter in tokamak research is the radial scale length of plasma turbulence, since it is directly related to the problem of anomalous transport. In Refs. 25 and 88, it was observed that this parameter could be inferred from the characteristics of waves reflected from closely spaced cutoff layers (Correlation Reflectometry). Based on the above model of reflectometry and on the assumption that $\tilde{\phi}$ is a normal random variable with normalized correlation $\gamma_\phi = \exp(-x^2/2\delta_x^2 - y^2/2\delta_y^2 - t^2/2\delta_t^2)$, the spectral coherence for waves reflected from two closely spaced cutoff layers is[91]

$$\gamma_E(\Delta x_c) \equiv \frac{<\tilde{E}_1(k_y,\omega)\tilde{E}_2^*(k_y,\omega)>}{<|\tilde{E}_1(k_y,\omega)|^2>}$$

$$= \frac{\sum_{n=1}^{\infty} (\sigma_\phi^{2n}/nn!)\exp(-nx^2/2\delta_x^2)\exp(-k_y^2\delta_y^2/2n)\exp(-\omega^2\delta_t^2/2n)}{\sum_{n=1}^{\infty} (\sigma_\phi^{2n}/nn!)\exp(-k_y^2\delta_y^2/2n)\exp(-\omega^2\delta_t^2/2n)} \ , \qquad (39)$$

where Δx_c is the separation of the cutoff layers, and $\tilde{E} = E - <E>$ is the random component of the scattered field. For $k_y \approx 0$ and $\omega \approx 0$, we obtain

$$\gamma_E \approx \frac{\mathrm{Ei}(\sigma_\phi^2\gamma_x) - \xi - \ln(\sigma_\phi^2\gamma_x)}{\mathrm{Ei}(\sigma_\phi^2) - \xi - \ln(\sigma_\phi^2)} \ , \qquad (40)$$

where Ei is the exponential integral,[99] $\xi = 0.577$ is the Euler number, and $\gamma_x = \exp(-x^2/2\delta_x^2)$ is the *x*-component of γ_ϕ. In the limit of $\sigma_\phi^2 << 1$, we arrive back at the linear or Born approximation where $\gamma_E \approx \gamma_x$, while for $\sigma_\phi^2 \gamma_x > 2.5$, from the asymptotic form of Ei we obtain

$$\gamma_E \approx \frac{1}{\gamma_x} \exp[-\sigma_\phi^2 (1-\gamma_x)] \ . \qquad (41)$$

Thus for sufficiently large σ_ϕ the value of the signal correlation may be much smaller than the corresponding value of γ_x. By expanding γ_x to the second order in x it is readily shown that $\gamma_E \approx \exp(-x^2 \sigma_\phi^2 / 2\delta_x^2)$, so that the correlation length of the measured signal is a factor of σ_ϕ smaller than the correlation length of the phase. It may also be shown numerically from Eq. (39) that the same is true for the *y*-correlation length, as discussed earlier in this Section, and for the correlation time.

Recently, a direct comparison between the radial correlation length of turbulent fluctuations as measured by Langmuir probes and correlation reflectometry was performed on the CCT tokamak at UCLA.[92] The published results show good agreement between the two diagnostics, with radial correlation lengths in the range 1-3 cm. According to the above model of reflectometry, such an agreement requires a value of $\sigma_\phi^2 << 1$ (not given in Ref. 92), so that $\gamma_E \approx \gamma_x$. Moreover, because of the small probing wavenumbers ($k_0 \approx 2$ cm-1) used in the experiment, the reflectometer could sample only fluctuations with $\Delta k_y << 1$, so that the close proximity of the receiving antenna to the reflecting layer (≈10 cm) made the phase of the measured signal a good representation of density fluctuations (Fig. 6). Nevertheless, the main conclusion that one could draw from these results, i.e., that correlation reflectometry can provide a direct measure of the scale of turbulent fluctuations even when it is smaller than the wavelength of the probing wave, cannot be supported by the model of reflectometry described in this Section, nor by a variety of numerical simulations.[91,112-116,120]

Figure 8 shows two examples of the measured spectral coherence at 0 and $k_y \approx 0$ as a function of the cutoff separation of two closely spaced reflectometer signals.[121] These results were obtained in the main core of TFTR discharges, where it was found that the ion mass modifies the transport of plasma, making discharges in Tritium better confined than those in Deuterium. The similarity of γ_E in the two cases of Fig. 8 strongly suggests that this phenomenon might not be caused by changes in the radial scale length of plasma turbulence. Nevertheless, one must stress that the spectral coherence in Fig. 8 is that of the mea-

sured signals - not the coherence of density fluctuations. In principle, using the model of reflectometry discussed in this Section, it is possible to obtain the latter from the measured γ_E if the properties of $\tilde{\phi}$ are known. For instance, the radial coherence of density fluctuations can be obtained from the data of Fig. 8 using Eqs. (34) and (39) and the value of σ_ϕ. Unfortunately, as explained above, the characteristics of $\tilde{\phi}$ cannot be inferred from the phase of the measured signal if the latter is detected in the far field region, as in most cases including that of Fig. 8. It is only by sampling the backward field at the virtual cutoff location that it is possible to reconstruct the field of turbulent fluctuations. Experimentally, this could be achieved by collecting the reflected waves with a wide aperture antenna, and by imaging the virtual cutoff onto an array of phase sensitive detectors. Such a reflectometry scheme, that is reminiscent of that described in Ref (73), is very demanding in terms of plasma accessibility. Nevertheless, it has the potential for providing additional information on the nature of the short-scale turbulence observed in tokamaks, which still remains an outstanding crucial issue.

V. INSTRUMENTATION AND TECHNIQUES

A reflectometer system is made of three major components: a microwave source, a transmission line, and a detection system. In this Section, we will discuss the main features of this hardware, emphasizing those aspects which are of importance for the application of this technique to a fusion reactor.

As discussed in the previous Sections, reflectometry measurements require the use of multiple frequencies, either in sequence or simultaneously. In early reflectometers, backward-wave-oscillators (BWO) were used as tunable sources of radiation. In these tubes, where microwave beams are generated by electrons moving inside a slow-wave structure[122], the wave frequency is proportional to the electron velocity, and thus it can be changed by controlling an applied voltage. The main advantage of BWOs is their wide range of tunability, which can be the entire microwave band of operation, and a relatively large output power, which can be in excess of 100 mW at 140 GHz. More recently, BWOs have been replaced by solid state Gunn diodes[122] which offer the advantage of a better frequency stability, a lower noise, a long life, and require low voltages and hence simpler power supplies. The frequency range of these oscillators (≈18-140 GHz) is determined by the structure of the semiconductor and the applied voltage. Even though their range of tunability extends over less than 1% of the center frequency, when used in combination with a varactor diode their range of electrical tunability can rise to ≈10% of center frequency, with power levels in

the range of 10-100 mW. Finally, the frequency can be extended by frequency multipliers (doublers, triplers, and quadruplers) spanning the range 18-600 GHz, with output powers ranging from 50 mW at the lower frequencies, to 0.1 mW at 600 GHz.

The use of low power reflectometers in large experiments, where most diagnostic systems must be located at a large distance from the plasma, requires the use of transmission lines with very low losses. A common solution is the use of oversized waveguides, as in the O-mode reflectometer of the Joint European Torus (JET)[16-19,48] which employs 25 m long WR187 (C-band) copper waveguides with the TE_{01} mode of propagation in the frequency band 18-80 GHz, and a total loss of ≈10 dB. In the X-mode reflectometer of the Tokamak Fusion Test Reactor (TFTR)[91,123] operating in the frequency range 110-140 GHz, a low transmission loss is instead achieved using cylindrical corrugated waveguides with the HE_{11} mode, where losses are not only very low, but are also insensitive to misalignments and deformations.[125] As a result, the power loss in the TFTR aluminum waveguides, which have a length of 15 m and a diameter of 6.35 cm, is less than 1 dB.

The simplest reflectometer circuit is illustrated by the block diagram of Fig. 9, where a wave with a constant amplitude and angular frequency ω_0 is launched into the plasma where it is reflected back and scattered. The portion which is captured by the receiving antenna produces the signal $s(t) = a(t)\cos(\omega_0 t + \phi(t))$, with the amplitude $a(t)$ and a the phase $\phi(t)$ that are slowly varying functions of time on the scale ω_0^{-1}. The frequency $\omega_r = d\phi(t)/dt$ can be interpreted as the instantaneous Doppler shift of the received wave, and thus $|\omega_r| << \omega_0$. As discussed in the previous Sections, in the absence of density fluctuations the amplitude a is almost constant, and the phase delay $\phi(t)$ carries information on the position of the reflecting layer. In the presence of density fluctuations, both $a(t)$ and $\phi(t)$ contain a stochastic component that carries information on the statistical properties of fluctuations.

In the block diagram of Fig. 9, the signal s is mixed with a portion of the transmitter output in mixer M1, and the resulting signal is filtered by a low-pass-filter (LPF) with cutoff frequency $\omega_c > |\omega_r|$. The sign of ω_r is lost unless the signal is processed with the digital equivalence of heterodyne detection. Another disadvantage of this scheme is that its dynamic range may be limited by the transmitter AM noise, and by the mixer noise. To avoid these drawbacks, one can use the heterodyne detection scheme of Fig. 10, where the output of the microwave oscillator O1 with frequency $\omega_1 (\approx \omega_0)$ is used as a local oscillator (LO) for

downshifting the frequency of both the received and the reference signals. A typical value for the IF frequency $(\omega_0 - \omega_1)/2\pi$ is ±500 MHz. To compensate for frequency jitters and drifts in the microwave source, one may add the intermediate frequency (IF) stage[125] of Fig. 11, which employs as LO a stable crystal controlled oscillator (O2) with frequency ω_2 in the range $|\omega_r| << \omega_2 < |\omega_0 - \omega_1|$. One sideband from the mixer M2, where O2 is mixed with the reference signal of Fig. 10, is filtered by a narrow band-pass-filter (BPF) and it is combined in M1 with the signal from the circuit of Fig. 10, to produce a new signal at frequency $\omega_2 - \omega_r$. Full information on the spectral characteristics of the received signals can then be obtained with standard numerical techniques using the quadrature detection scheme of Fig. 12 together with two signal digitizes

The range of tunability of this reflectometer scheme is limited by the BPF band on the output of M1 in Fig. 11, which is typically of the order of 100 MHz. Thus its use for density profile measurements or for density fluctuations requires a multi-channel system for spanning the frequency range of interest. This approach has been adopted in the O-mode reflectometer of JET16-1[9,48] where 12 independent sources (Gunn oscillators) with frequencies in the range 18-80 GHz are launched through a single oversized waveguide. The frequency of each source is swept in 3-6 ms over a narrow band of ≈100 MHz, providing the group delay at 12 radial locations. In this reflectometer, the IF stage of Fig. 11 is replaced by a phase-lock loop which maintains $|\omega_0 - \omega_1|$ to a constant value of 10.7 MHz. Figure 13 shows an example of the measured density profiles in JET, which appears to be in good agreement with the profiles obtained from Thomson scattering and infrared interferometry.[48]

The reflectometer scheme of Figs. 10 and 11 can be easily modified to extend its range of tunability. This is illustrated in Fig. 14, where the circuit of Fig. 10 is modified to include a tunable transmitter in the frequency range $\omega_a < \omega_0 < \omega_b$, and two LOs with frequencies ω_1 and ω_2, that are used for producing a main signal at $\omega_2 - \omega_1 + \omega_r$, and a reference signal at $\omega_2 - \omega_1$. This circuit can then be combined, as before, with the IF stage of Fig. 11 and the quadrature detection scheme of Fig. 12. A multi-channel reflectometer of this type, using the X-mode in the frequency band 110-140 GHz, was used for studying turbulent fluctuations in TFTR.[91,119,121]. Some of the results have been given in Figs. 5 and 8. Another is displayed in Fig. 15, which shows the frequency dependence of the common power P_E and the spectral coherence γ_E of two reflectometer signals with a cutoff separation of $\approx 2\pi / k_0$.

One of the main reasons for using heterodyne detection, in spite of its complexity, is the preservation of the sign of phase variations. As mentioned above, this can be achieved with homodyne detection as well (Fig. 9) if the signal is processed with the digital equivalence of heterodyne detection: the Complex Demodulation Method (CDM).126 Suppose in fact that the signal from a reflectometer with the simple detection scheme of Fig. 9 is , where δ is an initial phase. If then the digitized signal is multiplied by the complex modulation $2\exp(-i\omega_m t)$ with $\omega_m \approx \omega_s$, and it is filtered by a low-pass digital filter with cutoff frequency $\omega_c < \omega_m$, the result is

$$s(t) = a(t)e^{i(\omega_S - \omega_m)t + i\delta} \ , \qquad (42)$$

from which can be easily derived. This method is currently employed for density measurements on the DIII-D tokamak,[68,76] with a reflectometer comprising two X-mode subsystems, one operating in Q-band (33-50 GHz) for edge density measurements, and the other in V-band (50-75 GHz) for central density measurements. An example of a measured density profile is displayed in Fig. 16 together with the corresponding Thomson scattering data.[71]

One of the major difficulties in performing density measurements with reflectometry is the spurious effect of density fluctuations. Formally, we can cast the phase of the measured signal

$$\phi(t) = \overline{\phi}(\omega_0(t)) + \tilde{\phi}(t, \omega_0(t)) \ , \qquad (43)$$

as the sum of a monotonic phase delay $\overline{\phi}$, resulting from the sweeping of the input frequency ω_0, and the contribution of fluctuations $\tilde{\phi}$. When $|\tilde{\phi}| << \pi$, the phase delay $\overline{\phi}$, from which one can infer the plasma density profile, is easily obtained by averaging ϕ over time and frequency sweeps. Unfortunately, in the opposite limit where $|\tilde{\phi}| \geq \pi$, this becomes very difficult, if not impossible. Particularly dangerous are 2D density fluctuations, which as explained in Sec. IV may transform the reflected signal in the far field region into a Gaussian noise, and thus with a phase which is uniformly distributed in the interval $(-\pi, \pi)$. To compensate in part for these spurious effects, single frequency reflectometer systems, such as the DIII-D reflectometer of the previous paragraph, employ very fast frequency sweeps (10-100 ms), so that the IF frequency broadening caused by fluctuations becomes smaller than the IF frequency itself. The results are then averaged over several sweeps. A better solution is offered by two-frequency reflectometer schemes,[14,35,37 where tw]o microwave beams with a constant frequency separation $\delta\omega_0$ are simultaneously

injected into the plasma and the phase difference is measured while the frequencies are swept across the band of interest. Then if $\delta\omega_0$ is chosen to make $|\delta\tilde{\phi}|<1$, $\delta\bar{\phi}$ can be obtained from the time average of $\delta\phi$. To derive the conditions for a two-frequency reflectometer, we consider the limit of large fluctuations, where the two complex signals s_1 and s_2 have zero mean, as in the case of Fig. 15. The distribution of is then given by

$$P(\delta\tilde{\phi}) = \frac{1-\gamma_s^2}{2\pi}\Big[\frac{\gamma_s\cos(\delta\tilde{\phi})}{(1-\gamma_s^2\cos^2(\delta\tilde{\phi}))^{3/2}}\Big(\frac{\pi}{2}+\sin^{-1}(\gamma_s\cos(\delta\tilde{\phi})\Big)+\frac{1}{1-\gamma_s^2\cos^2(\delta\tilde{\phi})}\Big], \quad (44)$$

which is displayed in Fig. 17 for several values of the normalized cross-correlation $\gamma_s \equiv <s_1 s_2^*> / <|s_1|^2>$. This figure shows how $P(\delta\tilde{\phi})$ goes from a uniform distribution ($=1/2\pi$) for $\gamma_s \approx 0$, to a delta function for $\gamma \approx 1$. For the case of Fig. 15, where $\gamma_s \approx 0.9$, we get $<|\delta\tilde{\phi}|^2>^{1/2} \approx 0.6$, which is not only smaller than one, but it is also much smaller than the value of $\delta\bar{\phi} > 2\pi$ that corresponds to the cutoff separation. In general, taking $\gamma_\phi(\xi) = \exp[-(\xi/\Delta)^2]$ for the normalized autocorrelation of the phase of geometric optics, and following the same arguments as in Sec. IV, we get that the cutoff separation δ for $\gamma_s \approx 0.9$ is given by

$$\frac{\delta}{\Delta} \approx \frac{1}{3\sigma_\phi}, \quad (45)$$

where, as before, σ_ϕ^2 is the variance of the phase of geometric optics (not the phase of the measured signal). For TFTR,[91,127] taking $\sigma_\phi \approx 3$ rad and Δ=1-2 cm, we obtain δ=0.1-0.2 cm.

One approach to two-frequency reflectometry[14,35] is illustrated in Fig. 18, where the output of the tunable microwave oscillator O1 with frequency ω_0 is modulated in amplitude at frequency Ω (typically 100-400 MHz). This produces three spectral components at and , that are reflected by the plasma with Doppler shifts ω_r and $\omega_{r\pm}$, respectively. The received signal is then measured by the square-law detector D1, and filtered by a BPF with a frequency band $\Delta\Omega$ in the range $|\omega_{r\pm}| << \Delta\Omega << \Omega$. The wave group delay is then obtained from the phase delay with respect to the modulating signal The main disadvantage of this scheme is its sensitivity to spurious reflections. Figure 19 shows an example of density profile on the outer part of a PBX-M tokamak plasma,65 measured with an amplitude modulation reflectometer using the X-mode in the frequency range 32-50 GHz, and with $\Omega/2\pi$=200 MHz.

Another approach to two-frequency reflectometry[37] is illustrated in Fig. 20, where two tunable microwave beams with constant frequency separation are simultaneously injected into the plasma. The two

beams are produced with the scheme of Fig. 21, together with a third locked beam that is used as the local oscillator in mixer M1 of Fig. 20, where the two reflected waves with frequencies $\omega_{01}+\omega_{r1}$ and $\omega_{02}+\omega_{r2}$ are detected. The two components of the output of M1 are then separated using two BPFs, and are recombined in mixer M3 to produce a signal with the frequency $\omega_{02}-\omega_{01}+\omega_{r2}-\omega_{r1}$, from which the wave group delay is finally obtained. Figure 22 shows an example of TFTR density profile,[58,59] measured with a two-frequency reflectometer operating in the band 90-118 GHz with the X-mode, and a frequency separation of 125 MHz.

Finally, it is worth mentioning the scheme of pulse radar reflectometry, where the wave group delay is obtained from the time of flight of short pulses. In one version of this method,[33,34,36,46,49,62] a short electromagnetic pulse is launched directly into the plasma. Since each of its Fourier components is reflected from a different location inside the plasma, the pulse duration is chosen so that its frequency spectrum is sufficient to span the accessible plasma region. The density profile is then obtained from the measured time of flight of each spectral component. Numerical simulations[63,64] indicate that the reconstruction of density profiles from pulse reflectometry measurements is quite robust with respect to finite amplitude perturbations. The apparent simplicity of this method, where a single ultra short pulse replaces the multiple tunable sources of conventional reflectometry, makes it particularly suitable for density measurements in large devices, such as ITER. A proof-of-principle system using 65 ps pulses has been built and tested on the CCT tokamak at UCLA, giving results in agreement with other diagnostics.[74] The possibility of using nonlinear transmission lines for producing the ultra short pulses ($\approx$ 1-2 ps) that are needed for applying this technique to an ITER-type plasma is currently under investigation.[74]

In another approach to pulse radar reflectometry,[69] which can be considered the dual of the previous method, a set of discrete waves with frequencies within a band Δf are launched sequentially into the plasma. By applying the Fourier transform to the measured frequency dependence of the amplitude and the phase of reflected signals, one can reconstruct a pulse in the time domain and obtain the wave group delay. Since this is equivalent to launching a pulse of duration $\Delta t = 1/\Delta f$ that can be shorter than the physical time of the measurement, this method goes under the name of pulse compression radar reflectometry. Preliminary tests on JET plasmas[69] indicate that the complete density profile could be measured in 2 to 5 μs using available fast frequency synthesizers. As compared to the first scheme, this approach avoids the

need for ultra shorts pulses, but requires waves with multiple frequencies and needs a more complicated detection scheme.

VI. DISCUSSION

As discussed in the Introduction, microwave reflectometry possesses some of the characteristics of an ideal diagnostic for a fusion reactor. During the past ten years, this method has made gigantic strides, and nowadays find extensive use in many tokamaks for density measurements. The crucial question then is whether the plasma of a fusion reactor will be more difficult to diagnose with reflectometry than those of present experiments. Two potential difficulties for reflectometry in reactor plasmas, i.e., in hotter and bigger plasmas than those of existing tokamaks, is plasma absorption and turbulent fluctuations. The first problem was addressed in Sec. II, where it was shown that the R-wave cannot penetrate the center of a tokamak reactor when launched from the low field side. Therefore, microwave reflectometry will be forced to operate with the O-mode for central density measurements, and with the X-mode for edge densities measurements.

The second problem, i.e., the spurious effects of plasma fluctuations, can be assess only using the full scaling of turbulence parameters. These include space and time scale lengths and the total amplitude of fluctuations. Even though such scalings are not well known, we can make safe predictions by assuming the worst scenarios. The first is based on the *mixing length criterion,*[128] which predicts that the maximum level of turbulence is

$$\sigma_n \propto (\bar{k}\ L\ )^{-1}\ , \tag{46}$$

where $\bar{k}$ is the typical turbulence wavenumber and L is a plasma spatial scale, such as the minor radius. For the space-scale of turbulence, we may assume[128] either the *Bohm-scaling*

$$\bar{k}\ \propto L^{-1}\ , \tag{47}$$

or the *gyro-Bohm scaling*

$$\bar{k}\ \propto \rho^{-1}\ , \tag{48}$$

where $\rho \propto T^{1/2}/B$ is the ion Larmor radius, T is the plasma temperature, and B is the magnetic field. Finally, for the turbulence time-scale τ, we may use the *drift wave scaling*

$$\tau^{-1} \propto \frac{\bar{k}\rho}{L} v_{th} \ , \qquad (49)$$

where $v_{th} \propto T^{1/2}$ is a thermal velocity. From this equation, we get that τ scales either as BL^2/T, or as $L/T^{1/2}$. Since temperatures and magnetic fields of a fusion reactor are not much different from those of plasmas in present large tokamaks, we conclude that the time scale of turbulence in a fusion reactor must increase, and therefore frequency sweeping and signal time averaging will be easier to perform. From Eq. (34) and the above equations, we also conclude that the variance σ_ϕ^2 of the phase of geometric optics scales either as $(k_0 L)^2$ or as $(k_0 \rho)^2$. In both cases, the cutoff separation between the signals of a two-frequency reflectometer (Eq. (45)) remains practically unchanged, so that this type of reflectometer will not be confronted with new difficulties in a fusion reactor.

Plasma turbulence and its relationship to anomalous transport is one of the most important outstanding problems of tokamak research. The major obstacle to the development of a satisfactory theory of turbulence in tokamaks is the scarcity of the experimental data, that very seldom contain all essential information, such as the full spectrum of fluctuations and their spatial distribution, and that in the best of cases require a very long acquisition time. In hydrodynamics, on the contrary, many advances in the theory of turbulence have been stimulated by optical techniques capable of providing a relatively quick visualization of the turbulence flow. Microwave reflectometry could offer the opportunity for the development of similar techniques for the study of the micro-turbulence in tokamaks. A conceptual design for a possible scheme is displayed in Fig. 23, where a probing wave with the X-mode and the frequency of 120 GHz is launched into the plasma using two different cylindrical lenses (L_1 and L_2). Their role is to focus the wave onto the centers of the two principal curvatures of the cutoff surface, so that it can propagate almost perpendicularly to the magnetic surfaces. For the case considered in Fig. 23, which is that of a JET-like tokamak, the center of the poloidal curvature is at R=2.38 m, while that of the toroidal curvature is obviously at R=0. Since the former depends on the wave frequency, the position of L_2 must be adjustable. Outside the plasma, the backward wave is reflected by a semitransparent mirror *M*, and an image of the cutoff is formed onto the detector plane *P* by the spherical lens L_3. The electromagnetic field is then measured with an array of microwave detectors. This type of arrays is beginning to appear in the technical literature, as in Ref. 129 which describes a microwave video camera employing a focal plane array (4 rows of 64 elements) for the

detection of a human body thermal emission at 94 GHz. Each array element has a noise of 0.5-1 Kelvin when frames have a duration of 1/30 s. Another example of detector array can be found in Ref. 130, which describes the measurement of the electron cyclotron emission from a tokamak plasma using a wide-band 20-channel array in the frequency band 90-110 GHz. Finally, the electromagnetic distribution of the reflected wave can be obtained from the intensity of a set of fringes, which can be formed using as a reference the forward reflection from the mirror *M*. Alternatively, but with considerable more difficulty, the complex amplitude of the reflected field can be measured with an independent set of local oscillators. Even though the implementation of this reflectometer scheme presents serious difficulties, such as the need for a large port or for 2D arrays of detectors, it has the potential for providing crucial information for the development of a theory of plasma turbulence.

ACKNOWLEDGMENT

This work was supported by United States Department of Energy Contract No. DE-AC02-76-CHO-3073.

REFERENCES

[1]I. E. Tamm and A. D. Sakharov, in *Plasma Physics and the Problem of Controlled Thermonuclear Reactions,* edited by M. A. Leontovich (Pergamon, Oxford, 1961), Vol. 1, p. 1.

[2]I. H. Hutchinson, *Principles of Plasma Diagnostics*, (Cambridge University Press, Cambridge, 1987).

[3]V. L. Ginzburg, *The Propagation of Electromagnetic Waves in Plasmas*, (Pergamon Press, Oxford, 1964).

[4]K. G. Budden, *The Propagation of Radio Waves*, (Cambridge University Press, Cambridge, 1985).

[5]A. I. Anisimov, N. I. Vinogradov, V. E. Golant, and B. P. Konstantinov, Sov. Phys. Tech. Phys. **5,** 939 (1961).

[6]V. A. Anoshkin, V. E. Golant, B. P. Konstantinov, B. P. Poloskin, and O. N. Shcherbinin, Sov. Phys. Tech. Phys. **5,** 1370 (1961).

[7]J. L. Doane, E. Mazzucato, and G. L. Schmidt, Rev. Sci. Instrum. **52**, 12 (1981).

[8]A. Cavallo and R. Cano, Technical Report EUR-CEA-FC-1137 (Association EURATOM-CEA sur la Fusion, 1982).

[9]F. Simonet, Rev. Sci. Instrum. **56**, 664 (1985).

[10]F. Simonet, *Étude de la Réflectometrie Hyperfréquence*, (Thése de Doctorate D'État, Universite dé Nancy I, 1985).

[11]M. A. G. Calderón and F. Simonet, Int. J. Infrared Millimeter Waves **6**, 605 (1985).

[12]P. Millot and F. Simonet, in *Proceedings of the 14th European Conference on Controlled Fusion and Plasma Physics*, Madrid, 1987 (European Physical Society, Petit-Lancy, Switzerland, 1987), p. 1303.

[13]H. Bottolier and G. Ichtchenko, Rev. Sci. Instrum. **58**, 539 (1987).

[14]V. A. Vershkov and V. A. Zhuravlev, Sov. Phys. Tech. Phys. **32**, 523 (1987).

[15]C. A. J. Hugenholtz and A. J. Putter, in *Basic and Advanced Diagnostic Techniques for Fusion Plasmas,* edited by P. E. Stott (Commission of the European Communities, Brussels, 1986), p. 469.

[16]A. E. Hubbard, A. E. Costley, J. A. Fessey, R. Prentice, and D. Ward, ibid., 461.

[17]R. Prentice, A. E. Costley, J. A. Fessey, and A. E. Hubbard, ibid., p. 451.

[18]A. E. Hubbard, Ph. D. Thesis (University of London, 1987).

[19]A. E. Hubbard, A. E. Costley, and C. W. Gowers, J. Phys. E: Sci. Instrum. **20**, 423 (1987).

[20]T. Lahecka, W. A. Peebles, N. C. Luhmann, S. R. Burns, and E. Olsen, Rev. Sci. Instrum. **59**, 1620 (1988).

[21]E. Anabitarte, E. G. Bustamante, M. A. Calderón, and J. Senties, A. P. Navarro, and J. Sánchez, J. Phys. D: Appl. Phys. **21**, 1384 (1988).

[22]A. Buffa, P. Innocente, S. Martini, M. Moresco, E. Spada, and E. Zilli, in *Proceedings of the 16th European Conference on Controlled Fusion and Plasma Physics*, Venice, 1989 (European Physical Society, Petit-Lancy, Switzerland, 1989), p. 1493.

[23]M. E. Manso, F. Serra, J. Barroso, et al., ibid., p. 837.

[24]J. Sánchez, E. Anabitarte, A. P. Navarro, and H. J. Hartfuss, ibid., p. 1565.

[25]A. E. Costley, P. Cripwell, R. Prentice, and A. C. Sips, Rev. Sci. Instrum. **61**, 2823 (1990).

[26]E. J. Doyle, T. Lahecka, N. C. Luhmann, and W. A. Peebles, Rev. Sci. Instrum. **61**, 2896 (1990).

[27]J. H. Irby and P. Stek, Rev. Sci. Instrum. **61**, 3052 (1990).

[28]M. Manso, F. Serra, A. Silva, et al., in *Proceedings of the 17th European Conference on Controlled Fusion and Plasma Physics*, Amsterdam, 1990 (European Physical Society, Petit-Lancy, Switzerland, 1990), p. 1517.

[29]R. Prentice, A. C. C. Sips, J. A. Fessey, and A. E. Costley, ibid, p. 1500.

[30]R. Shubert, F. Braun, J. Gernhardt, et al., ibid., p. 1552.

[31]M. Manso, F. Serra, A. Silva, et al., ibid., p. 1560.

[32]C. A. J. Hugenholttz, Rijnhuizen Report 90-192 (FOM-Institut voor Plasmafysica Rijnhuizen, Nieuwegein 1990).

[33]C. A. Hugenholtz and S. H. Heijnen, Rev. Sci. Instrum. **62**, 1100 (1991).

[34]S. H. Heijnen, C. A. Hugenholtz, and P. Pavlo, in *Proceedings of the 18th European Conference on Controlled Fusion and Plasma Physics*, Berlin, 1991 (European Physical Society, Petit-Lancy, Switzerland, 1991), p. IV-309.

[35]J. Sánchez, B. Brañas, T. Estrada, E. de la Luna, and V. A. Zhuravlev, Rev. Sci. Instrum. **63**, 4654 (1992).

[36]C. W. Domier, E. Chung, E. J. Doyle, H. L. Liu, A. Lapidus, N. C. Luhmann, W. A. Peebles, X. H. Quin, T. L. Rhodes, and L. Sjogren, Rev. Sci. Instrum. **63**, 4666 (1992).

[37]G. R. Hanson, J. B. Wilgen, T. S. Bigelow, I. Collazo, and C. E. Thomas, Rev. Sci. Instrum. **63**, 4658 (1992).

[38]M. Moresco, R. O Dubhghaill, and Spada, Int. J. Infrared Millimeter Waves **12**, 609 (1992).

[39]R. N. O Dubhghaill, D. R. Vizard, B. N. Lyons, and M. C. Sexton, Int. J. Infrared Millimeter Waves **13**, 309 (1992).

[40]S. H. Heijnen, C. A. J. Hugenholtz, M. J. van de Pol, A. Silva, M. E. Manso, F. Serra, et al., in *Proceedings of the 19th European Conference on Controlled Fusion and Plasma Physics*, Innsbruck, 1992 (European Physical Society, Petit-Lancy, Switzerland, 1992), p. 1059.

[41]A. Silva, M. E. Manso, F. Serra, et al., ibid., p. 1063.

[42]J. Sánchez, V. Zhuravlev, E. de la Luna, T. Estrada, and B. Brañas, ibid., p. 1075.

[43]M. E. Manso, Plasma Phys. Controll. Fusion **35**, B141 (1993).

[44]J. H. Irby, S. Horne, I. H. Hutchinson, and P. C. Stek, Plasma Phys. Controll. Fusion **35**, 601 (1993).

[45]A. Silva, M. E. Manso, P. Varela, F. Serra, L. Cupido, M. Albrecht, F. X. Söldner, and the ASDEX-U team, in *Proceedings of the 20th European Conference on Controlled Fusion and Plasma Physics*, Lisbon, 1993 (European Physical Society, Petit-Lancy, Switzerland, 1993), p. 1107.

[46]S. H. Heijnen, M. de Baar, M. J. van de Pol, and C. A. J. Hugenholtz, ibid., p. 1143.

[47]E. de la Luna, V. Zhuravlev, B. Brañas, J. Sánchez, T. Estrada, J. Segovia, and J. L. Oramas, ibid., p. 1159.

[48]A. C. Sips and G. J. Kramer, Plasma Phys. Control. Fusion **35**, 743 (1993).

[49]V. F. Shevchenko, A. A. Petrov, and V. G. Petrov, Int. J. Infrared Millimeter Waves **14**, 1755 (1993).

[50]C. Laviron, A. Costley, P. Millot, and R. Prentice, in *Proceedings of the 21th European Conference on Controlled Fusion and Plasma Physics*, Montpellier, 1994 (European Physical Society, Petit-Lancy, Switzerland, 1994) p. 1169.

[51]F. Clairet, M. Paume, and J. M. Chareau, ibid, p. 1172.

[52]V. Zhuravlev, B. Brañas, E. de la Luna, J. Sánchez, T. Estrada, and M. Francés, ibid., p. 1176.

[53]E. de la Luna, J. Sánchez, V. Zhuravlev, G. Hanson, J. Wilgen, B. Kaita, and the PBX-M team, ibid., p. 1180.

[54]L. Cupido, A. Silva, F. Serra, M. E. Manso, P. Varela, R. Prentice, and A. Costley, ibid., p. 1184.

[55]A. Silva, M. E. Manso, P. Varela, L. Cupido, et al., ibid., p. 1188.

[56]V. A. Vershkov, V. V. Dreval, and S. V. Soldatov, ibid., p. 1192.

[57]S. H. Heijnen, P. Pavlo, M. R. de Barr, et al., ibid., p. 1204.

[58]G. R. Hanson, J. B. Wilgen, T. S. Bigelow, I. Collazo, A. C. England, M. Murakami, D. A. Rasmussen, C. E. Thomas, J. R. Wilson, and H. K. Park, Plasma Phys. Control. Fusion **36**, 2073 (1994).

[59]G. R. Hanson, J. B. Wilgen, T. S. Bigelow, I. Collazo, A. C. England, M. Murakami, D. A. Rasmussen, and J. R. Wilson, Rev. Sci. Instrum. **66**, 863 (1995).

[60]E. Mazzucato and R. Nazikian, Rev. Sci. Instrum. **66**, 1237 (1995).

[61]M. Hirsh, T. Geist, H. J. Hartfuss, T. Estrada, and J. Sánchez, Rev. Sci. Instrum. **66**, 412 (1995).

[62]C. W. Domier, N. C. Luhmann, A. E. Chou, W. M. Zhang, and A. J. Romanowsky, Rev. Sci. Instrum. **66**, 399 (1995).

[63]B. I. Cohen, B. B. Afeyan, A. E. Chou, and N. C. Luhmann, Rev. Sci. Instrum **66**, 1241 (1995); Plasma Phys. Control. Fusion **37**, 329 (1995).

[64]B. I. Cohen, T. B. Kaiser, and J. C. Garrison, Rev. Sci. Instrum **68** 1238 (1997)

[65]E. de la Luna, J. Sánchez, V. Zhuravlev, I. García-Cortés, G. R. Hanson, J. B. Wilgen, et al., Rev. Sci. Instrum **66**, 403 (1995); E. de la Luna, G. Hanson, J. Sánchez,, J. B. Wilgen, V. A. Zhuravlev, M. Ono, and R. Kaita, Plasma Phys. Control. Fusion **37**, 925 (1995).

[66]M. Moresco, R. Cavazzana, A. Sardella, and E. Spada, Rev. Sci. Instrum **66**, 406 (1995).

[67]P. Buratti, M. Zerbini, Y. Brodsky, N. Kovalev, and A. Shtanuk, Rev. Sci. Instrum **66**, 409 (1995).

[68]K. W. Kim, E. J. Doyle, W. A. Peebles, A. Ejiri, N. C. Luhman, and C. L. Retting, Rev. Sci. Instrum. **66**, 1229 (1995).

[69]C. Laviron, P. Millot, and R. Prentice, Plasma Phys. Control. Fusion **37**, 975 (1995).

[70]C. Laviron, in *Proceedings of the International Workshop on Diagnostics for ITER*, Varenna, 1995 (Plenum Press, New York, 1996), p. 107.

[71]E. J. Doyle, K. W. Kim, J. H. Lee, W. A. Peebles, C. L. Retting, T. L. Rhodes, and R. T. Snider, ibid., p. 117.

[72]M. Manso, D. Bartlett, L. Cupido, W. Kasparek, J. Sánchez, P. Stott, and D. Wagner, ibid., p. 133

[73]V. A. Vershkov, ibid., p. 143.

[74]N. C. Luhmann, C. W. Domier, R. P. Hsia, and B. Deng, ibid., p. 171.

[75]C. Laviron, A. J. H. Donne, M. E. Manso, and J. Sánchez, Plasma Phys. Control. Fusion **38**, 905 (1996).

[76]K. W. Kim, E. J. Doyle, T. L. Rhodes, W. A. Peebles, C. L. Retting, and N. C. Luhman, Rev. Sci. Instrum. **68**, 466 (1997).

[77]E. Mazzucato, Bull. Am. Phys. Soc. **20**, 1241 (1975); Princeton University Plasma Physics Laboratory Report MATT-1151 (1975).

[78]E. Mazzucato, Phys. Rev. Lett. **36**, 792 (1976).

[79]C. M. Surko and R. E. Slusher, Phys. Rev. Lett. **37**, 1747 (1976).

[80]E. Mazzucato, Phys. Rev. Lett. **48**, 1828 (1982).

[81]D. L. Brower, W. A. Peebles, N. C. Luhmann, and R. L. Savage, Phys. Rev. Lett. **54**, 689 (1985).

[82]N. L. Bretz, E. Mazzucato, R. Nazikian, et al., in *Proceedings of Plasma Physics and Controlled Nuclear Fusion Research*, Würzburg, 1992 (IAEA, Vienna 1993) Vol. 1, p. 551.

[83]TFR Goup, Plasma Phys. Controll. Fusion **27**, 1299 (1985).

[84]P. Cripwell, A. E. Costley, and A. E. Hubbard, in *Proceedings of the 16th European Conference on Controlled Fusion and Plasma Physics*, Venice, 1989 (European Physical Society, Petit-Lancy, Switzerland, 1989), Vol. 12B, p. 75.

[85]E. J. Doyle, T. Lahecka, N. C. Luhmann, et al., Rev. Sci. Instrum. **61**, 3016 (1990).

[86]T. Estrada, J. Sánchez, B. Brañas, and A. P. Navarro, Rev. Sci. Instrum. **61**, 3034 (1990).

[87]G. R. Hanson, J. B. Wilgen, E. Anabitarte, et al., Rev. Sci. Instrum. **61**, 3049 (1990).

[88]P. Cripwell and A. E. Costley, in *Proceedings of the 18th European Conference on Controlled Fusion and Plasma Physics*, Berlin, 1991 (European Physical Society, Petit-Lancy, Switzerland, 1991), p. I-17.

[89]G. R. Hanson, J. H. Harris,J. B. Wilgen, et al., Nucl. Fusion **32**, 1593 (1992).

[90]E. Mazzucato, R. Nazikian, and the TFTR Group, in *Proceedings of the 19th European Conference on Controlled Fusion and Plasma Physics*, Innsbruck, 1992 (European Physical Society, Petit-Lancy, Switzerland, 1992), p. 1055.

[91]E. Mazzucato and R. Nazikian, Phys. Rev. Lett. **71** 1840 (1993).

[92]T. L. Rhodes, R. J. Taylor, and W. A. Peebles, Rev. Sci. Instrum. **66** 824 (1995).

[93]R. Nazikian and E. Mazzucato, Rev. Sci. Instrum. **66**, 392 (1995).

[94]G. D. Conway, L. Schott, and A. Hirose, Rev. Sci. Instrum. **67**, 3861 (1996); Plasma Phys. Control. Fusion **38**, 451 (1996).

[95]G. D. Conway, Plasma Phys. Control. Fusion **39**, 407 (1997).

[96]R. Aymar, V. Chuyanov, M. Huguet, R. Parker, and Y. Shimonura, in *Proceedings of the Sixteenth International Conference on Plasma Physics and Controlled Nuclear Fusion Research*, Montreal, 1996 (International Atomic Agency, Vienna, in press).

[97]S. Weinberg, Phys. Rev. **126**, 1899 (1962).

[98]I. B. Bernstein, Phys. Fluids **8**, 321 (1975).

[99]M.Abramowitz and I. A. Stegun, *Handbook of mathematical functions*, (Dover, New York, 1965).

[100]I. Fidone and G. Granata, Nucl. Fusion **11**, 133 (1971).

[101]M. Brambilla and M. Moresco, Plasma Phys. Control. Fusion **29**, 381 (1987).

[102]I. Fidone, G. Granata, and L. Meyer, Phys. Fluids **25**, 2249 (1982).

[103]M. Bornatici, R. Cano, O. De Barbieri, and F. Engelmannn, Nucl. Fusion **23,** 1153 (1983).

[104]D. B. Batchelor, R. C. Goldfinger, and H. Weitzner, Phys. Fluids **27**, 2835 (1984).

[105]M. Bornatici and U. Ruffina, Nuovo Cim. **6 D**, 231 (1985).

[106]I. Fidone and G. Granata, Phys. Plasmas **1**, 1231 (1994).

[107]H. Bindslev, Plasma Phys. Control. Fusion **33**, 1775 (1991).

[108]E. Mazzucato, I. Fidone, and G. Granata, Phys. Fluids **30**, 3745 (1987).

[109]E. Mazzucato, Phys. Fluids B **4**, 3460 (1992).

[110]E. M. I. Skolnik, *Introduction to Radar Systems*, (McGrow-Hill, New York, 1962).

[111]M. L. Pitteway, Proc. Roy. Soc. A **252**, 556 (1958).

[112]E. Mazzucato and R. Nazikian, Plasma Phys. Controlled Fusion **33**, 261 (1991).

[113]X. L. Zou, L. Laurent, and J. M. Rax, Plasma Phys. Controlled Fusion **33**, 903 (1991).

[114]I. H. Hutchinson, Plasma Phys. Controlled Fusion **34**, 1225 (1992).

[115]B. B. Afeyan, A. E. Chou, and B. I. Cohen, Plasma Phys. Controlled Fusion **37**, 315 (1995).

[116]N. Bretz, Phys. Fluids B **4**, 2414 (1992).

[117]S. O. Rice, Bell System Tech. J., **23**, 282 (1944); **24**, 96 (1945) (reprinted in N. Wax, *Selected Papers on Noise and Stochastic Processes* (Dover, New York, 1954)).

[118]P. Beckmann and A. Spizzichino, *The Scattering of Electromagnetic Waves from Rough Surfaces* (The Macmillan Company, New York, 1963).

[119]E. Mazzucato, S. H. Batha, M. Beer, M. Bell, R. E. Bell, R. V. Budny, C. Bush, T. S. Hahm, G. W. Hammett, F. M. Levinton, R. Nazikian, H. Park, G. Rewoldt, G. L. Schmidt, E. J. Synakowski, W. M. Tang, G. Taylor, and M. C. Zarnstorff, Phys. Rev. Lett., **77**, 3145 (1996).

[120]E. Mazzucato, to be published in Rev. Sci. Instrum.

[121]E. Mazzucato, R. Nazikian, S. Scott, and the TFTR Group, in *Proceedings of the 22nd European Conference on Controlled Fusion and Plasma Physics*, Bournemouth, 1995 (European Physical Society, Petit-Lancy, Switzerland, 1995), Vol. IV, p. 109

[122]T. Koryu Ishii, *Practical Microwave Electron Devices*, (Academic Press, San Diego, 1990).

[123]M. McCarthy, E. Mazzucato, A. Nagy, and R. Nazikian, in *Proceedings of the 14th Symposium on Fusion Engeneering*, San Diego, 1991 (), p. 1992.

[124]J. L. Doane, in *Infrared and Millimeter Waves*, edited by K. J. Button (Academic Press, New York, 1985), Vol. 13, p. 123.

[125]J. L. Doane, Rev. Sci. Instrum. **51**, 317 (1980).

[126]P. Y. Ktonas and N. Papp, Signal Process. **2**, 373 (1980).

[127]R. Fonck, G. Cosby, R. Durst, S. Paul, N. Bretz, S. Scott, E. Synakowski, and G. Taylor, Phys. Rev. Lett. **70**, 3736 (1993).

[128]W. Horton, Institute for Fusion Studies Report 798, (1997).

[129]G. C. Huguenin, SPIE **2938**, 152 (1996).

[130]R. P. Hsia, B. H. Deng, W. R. Geck, C. Liang, C. W. Domier, N. C. Luhmann, D. L. Brower, and G. Cima, *et al.*, Rev. Sci. Instrum. **68**, 488 (1997).

FIGURE CAPTIONS

Fig. 1. Characteristic plasma frequencies on the equatorial plane of an ITER-like plasma: $f_c = \omega_c / 2\pi$, $f_{2c} = 2 f_c$, $f_O = \omega_O / 2\pi$, $f_R = \omega_R / 2\pi$, $f_L = \omega_L / 2\pi$, f_{uh} is the upper-hybrid frequency.

Fig. 2. Electron density (dash) and temperature (solid) profiles on the equatorial plane of an ITER-like plasma.

Fig. 3. R-cutoff surfaces for *f*=185 GHz and the plasma parameters of Fig. 2; solid line is from the relativistic theory, dot-line is from the cold approximation. Also shown is the ray trajectory of a wave launched perpendicularly to the magnetic field from the low-field side of the torus with the X-mode.

Fig. 4. Fraction of total absorbed power versus frequency for a probing R-wave and the conditions of Figs. 2 and 3.

Fig. 5 Measured amplitude distribution of reflected signals in the far field region of a TFTR discharge. Solid line is from an X-mode reflectometer with phase quadrature detection. Circles are from the best fit of experimental data with a Rice distribution. Top is for reflection from the plasma center; bottom is for reflection from $r / a \approx 0.3$. (*From Ref. 119*)

Fig. 6 Calculated amplitude (top) and phase (bottom) of the reflected field at the cutoff virtual location for *f*=75 GHz and O-mode. Dashed line is the phase of geometric optics. The density profile is that of a typical TFTR discharge, and the density fluctuations are in the range Δk_x=1 cm^{-1}, Δk_y=0.5 cm^{-1}, and $\sigma_n = 5\text{x}10^{-3}$ (From Ref. 120)

Fig. 7 Same as in Fig. 6 at the plasma boundary. (*From Ref. 120*)

Fig. 8 Coherence γ_E ($\omega \approx 0$, $k_y \approx 0$) of two reflectometer signals (X-mode, ≈140 GHz) as a function of the cutoff separation Δr_c from the main core of TFTR discharges in Deuterium (top) and Tritium (bottom). Dash lines are Gaussian best fits. (F*rom Ref. 121*)

Fig. 9 Block diagram of a reflectometer with homodyne detection.

Fig. 10 Block diagram of a reflectometer with heterodyne detection.

Fig. 11 Block diagram of an IF stage for the compensation of frequency drifts in the circuit of Fig. 10.

Fig. 12 IQ phase detection scheme.

Fig. 13 Density profile measured with a multi-channel reflectometer in JET (circles); squares are interferometric data, and triangles are Thomson scattering data (*From Ref. 48*).

Fig. 14 Block diagram of a tunable reflectometer.

Fig. 15 Spectral coherence γ_E and common power P_E as a function of frequency for two reflectometer signals with a cutoff separation of $\approx 2\pi / k_0$. (*From Ref. 91*)

Fig. 16 Density profile obtained on DIII-D with a broadband, swept-frequency reflectometer using the CDM method (solid line); circles are Thomson scattering data. (*From Ref. 71*).

Fig. 17 Differential phase distribution for two Gaussian complex signals with variance $\sigma_s^2 = 1$, mean $< s >= 0$ and cross-correlation γ_s.

Fig. 18 Block diagram of an amplitude modulation reflectometer.

Fig. 19 Density profile obtained on PBX-M with an amplitude-modulation reflectometer: (a) measured differential phase as a function of frequency, and (b) corresponding reconstructed density profiles (solid line; crosses are Thomson scattering data . (*From Ref. 65*)

Fig. 20 Block diagram of a two-frequencies reflectometer.

Fig. 21 Block diagram for the production of two tunable microwave beams with constant frequency separation.

Fig. 22 Density profiles obtained on TFTR with a two-frequencies reflectometer: (a) measured differential phase as a function of frequency, and (b) corresponding reconstructed edge density profiles. (*From Ref. 58*)

Fig. 23 Conceptual design of a reflectometer apparatus for the visualization of turbulence in tokamaks; L_1 and L_2 are cylindrical lenses, L_3 is a spherical lens, M is a semitransparent mirror, and P is the plane of an array of detectors.

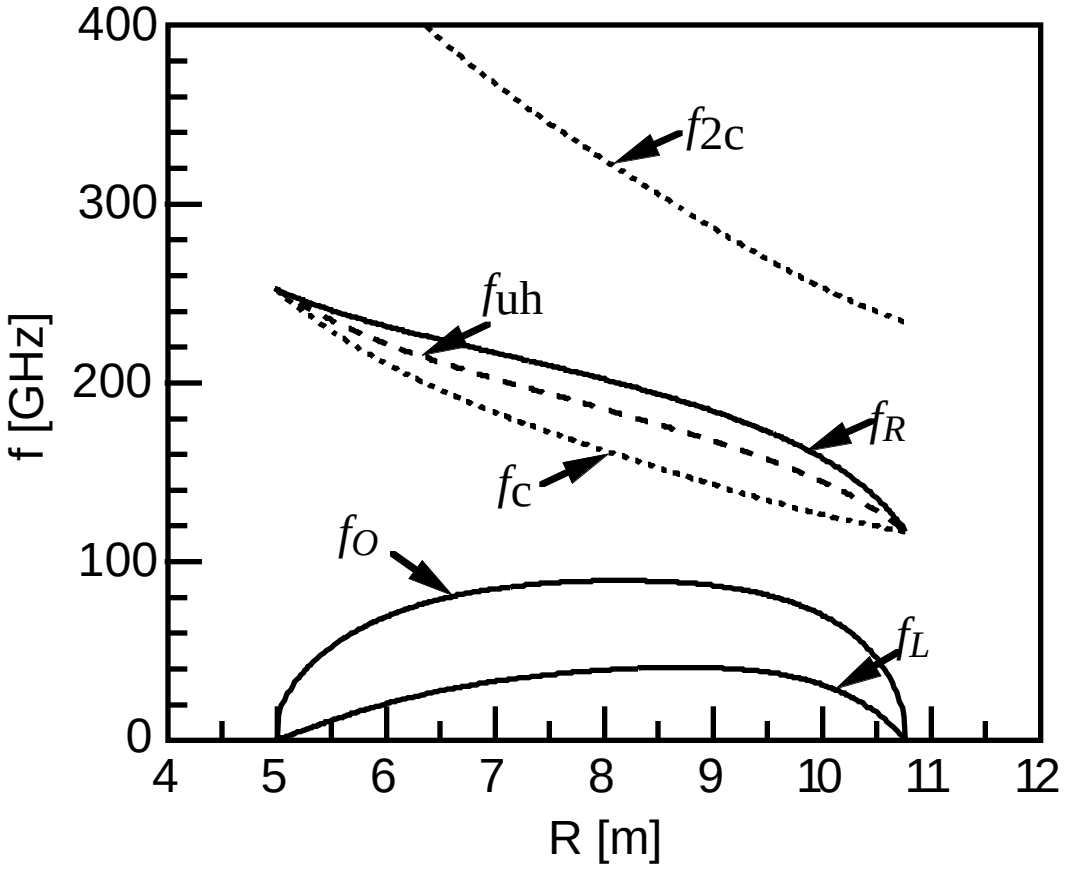

Fig. 1

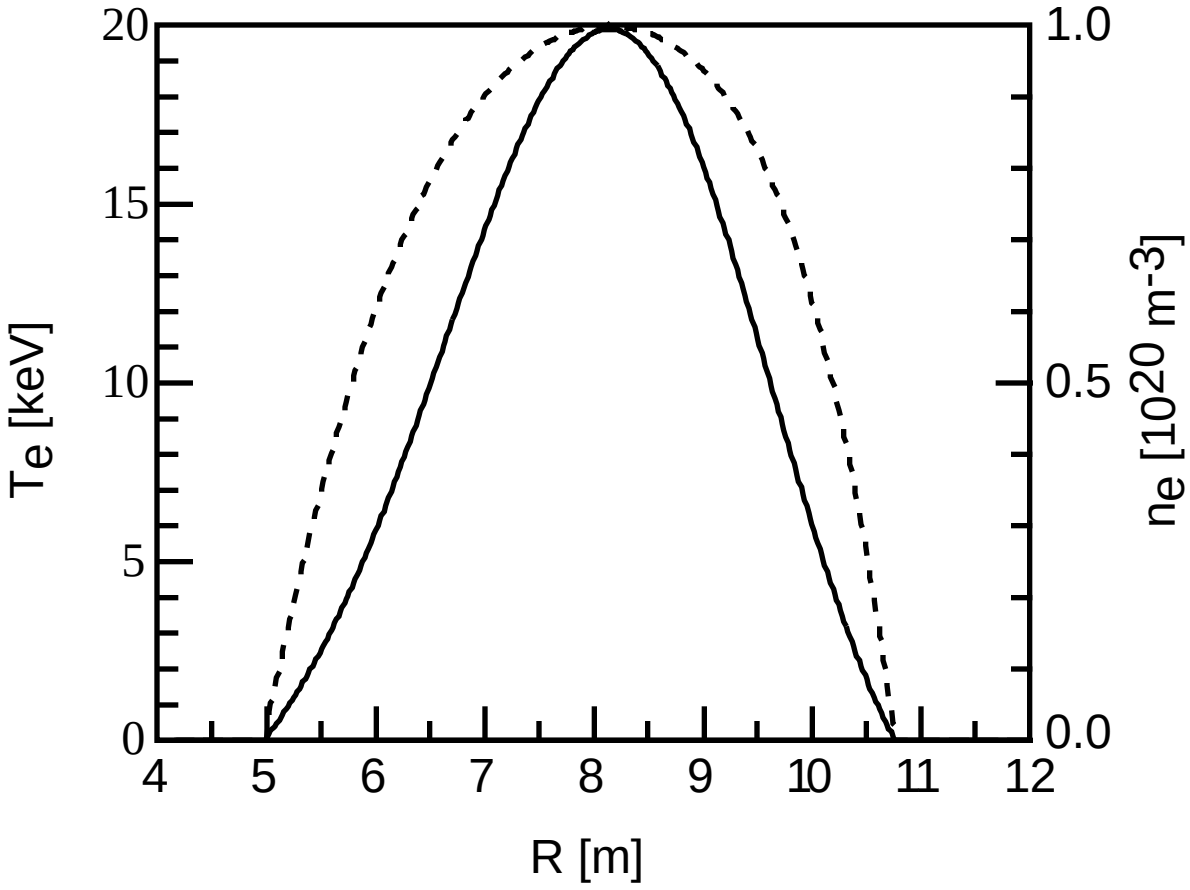

Fig. 2

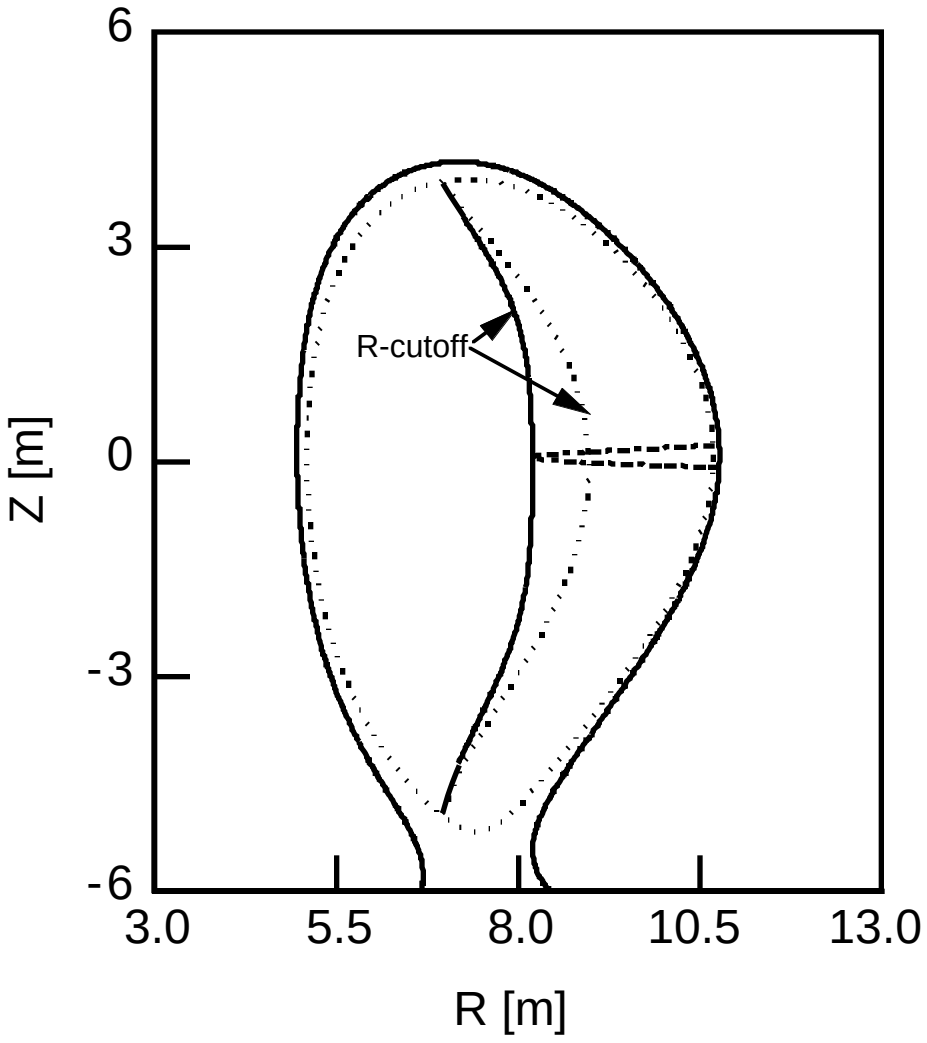

Fig. 3

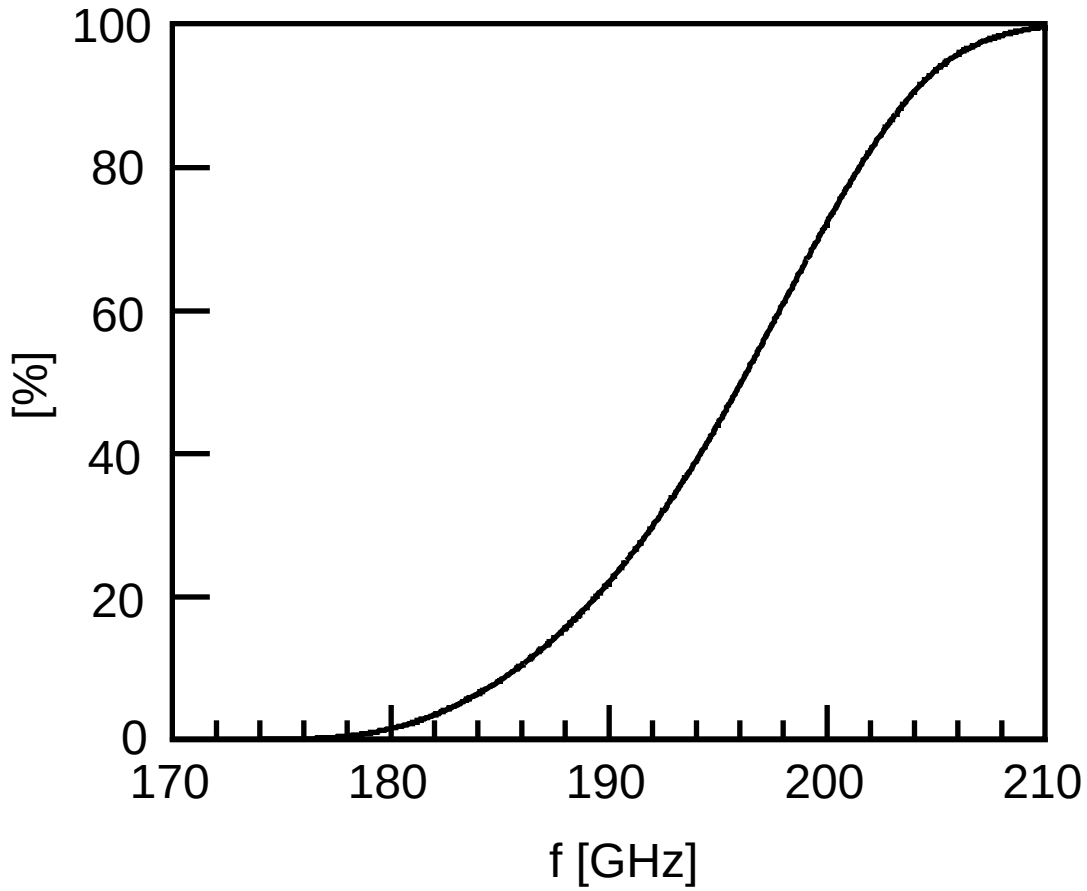

Fig. 4

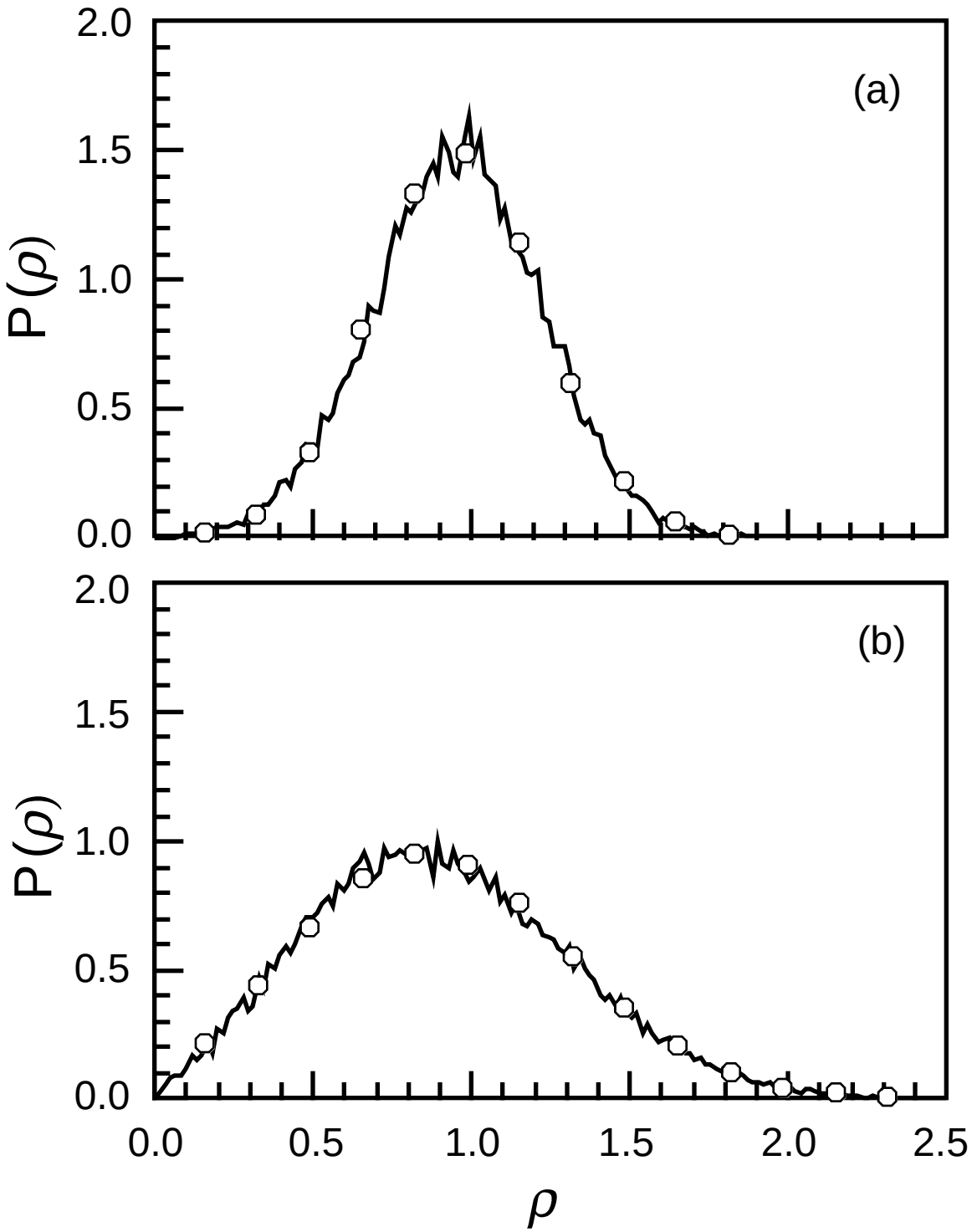

Fig. 5

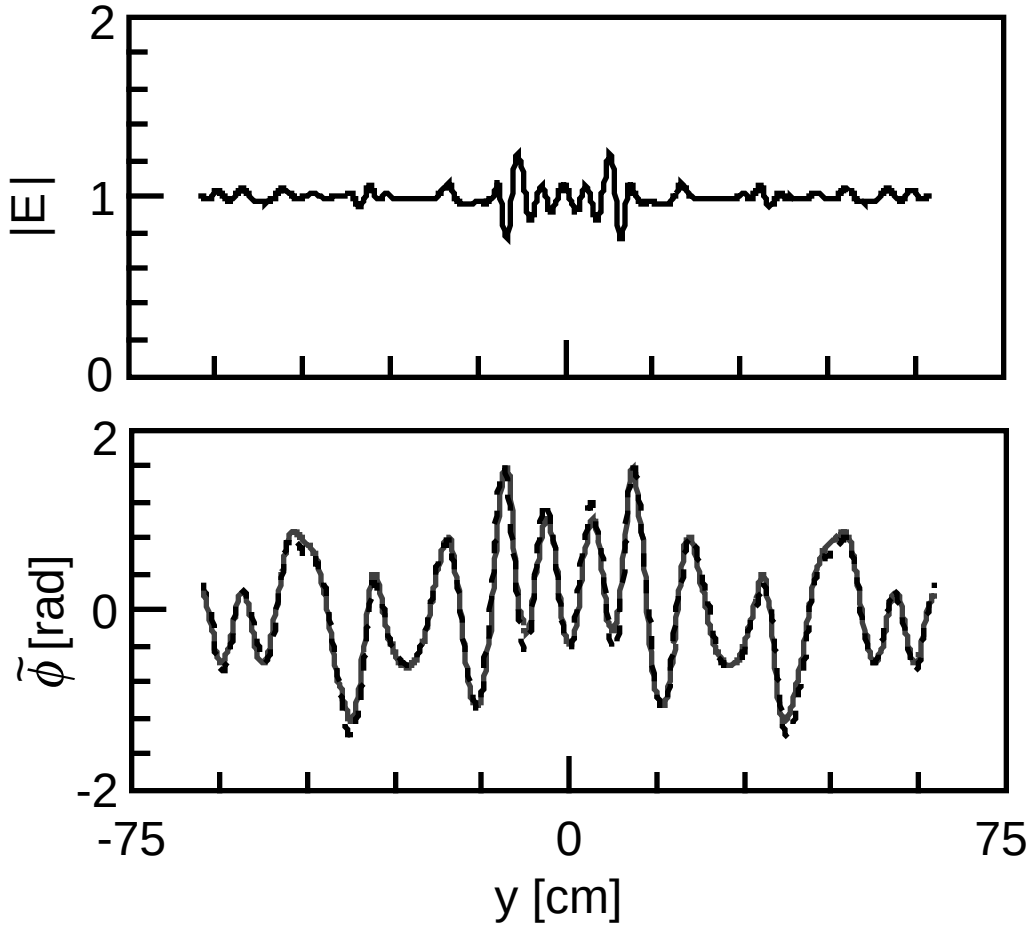

Fig. 6

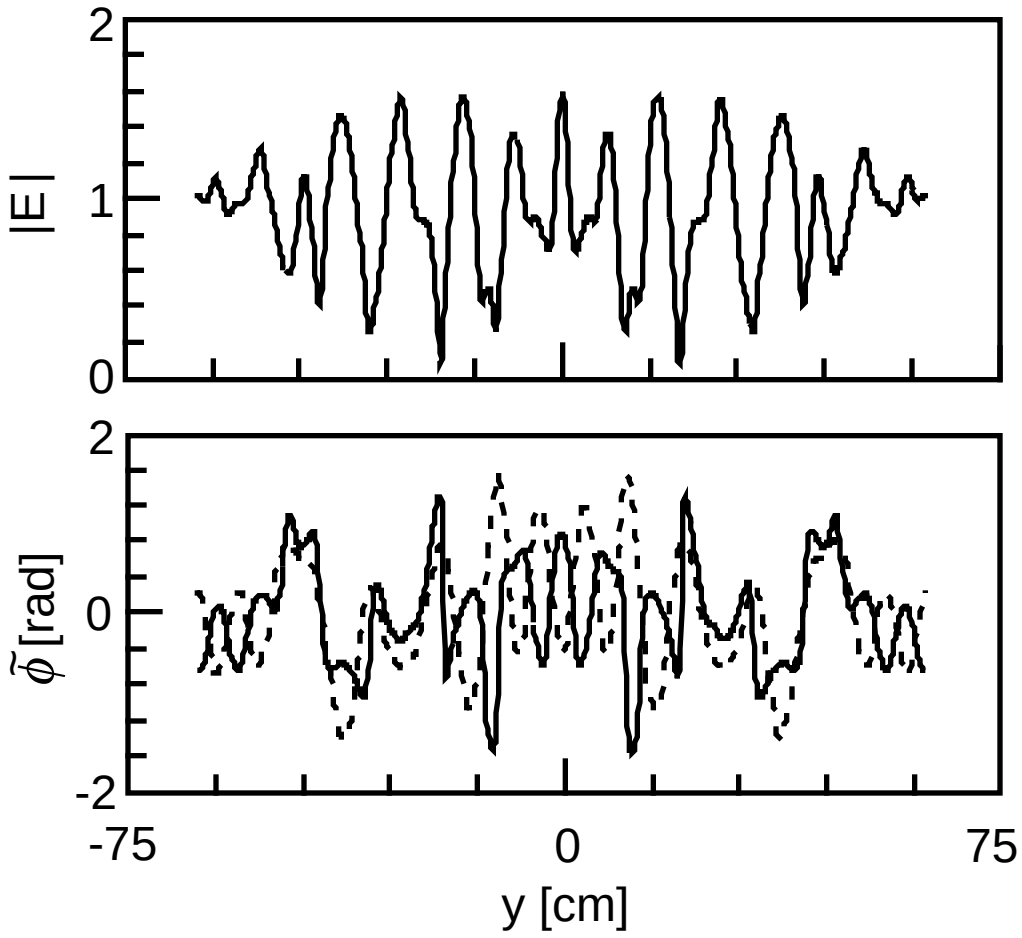

Fig. 7

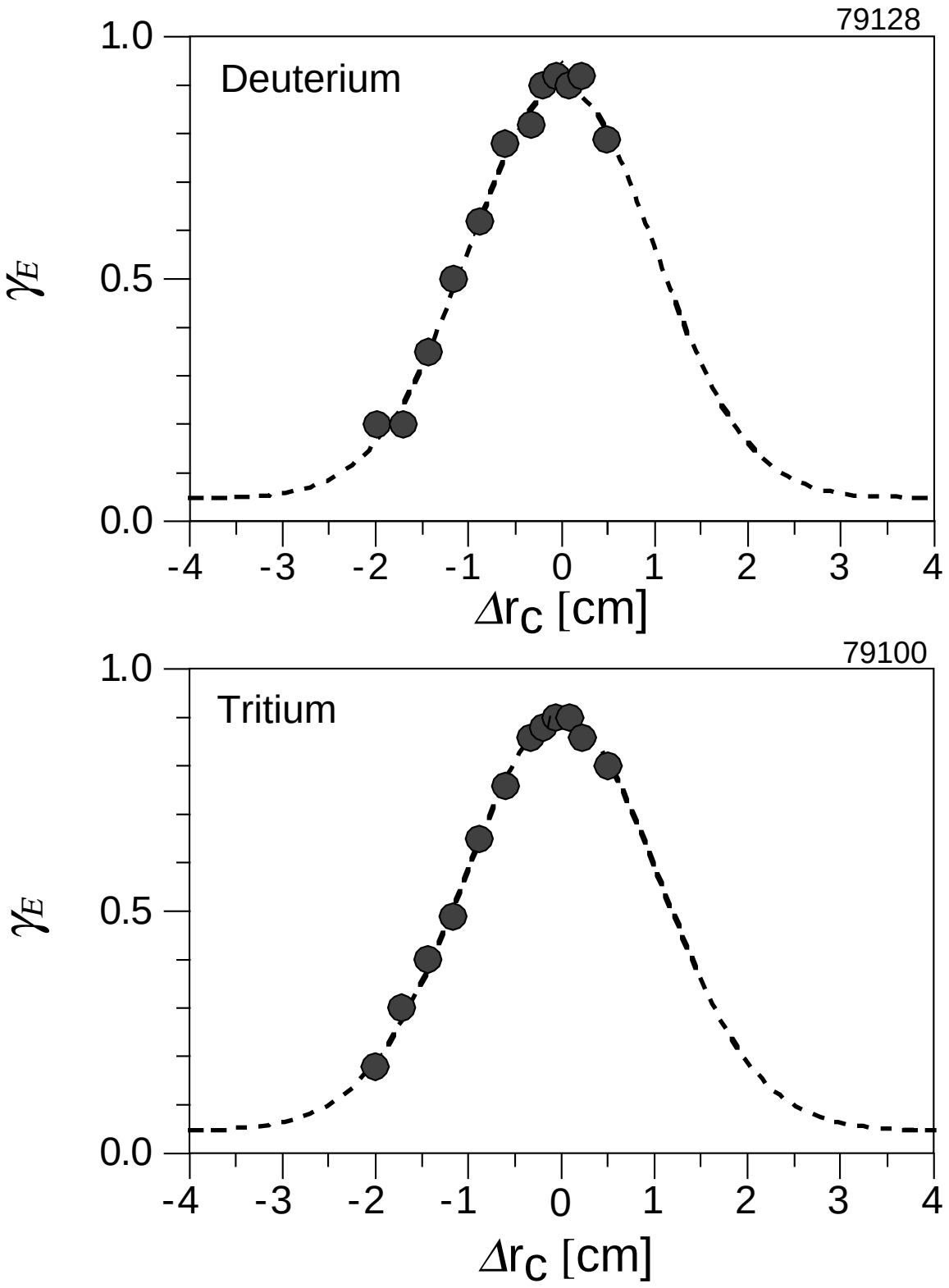
79128
Deuterium
1.0
0.5
0.0
γ_E
-4
-3
-2
-1
0
1
2
3
4
Δr_C [cm]
79100
Tritium
1.0
0.5
0.0
γ_E
-4
-3
-2
-1
0
1
2
3
4
Δr_C [cm]

Fig. 8

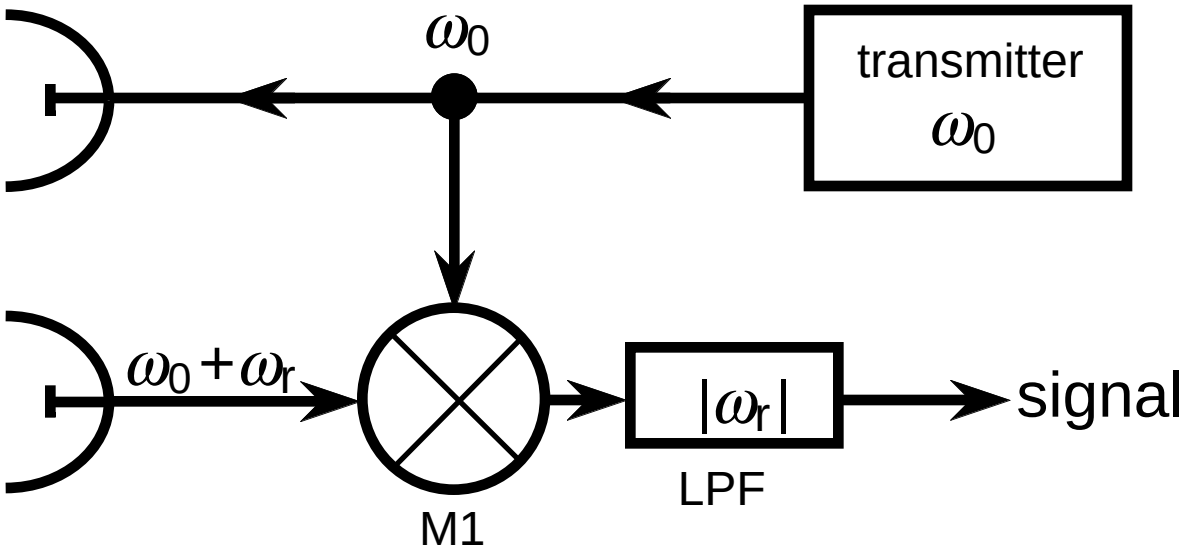
ω_0
transmitter
ω_0
$\omega_0+\omega_r$
$|\omega_r|$
signal
LPF
M1

Fig. 9

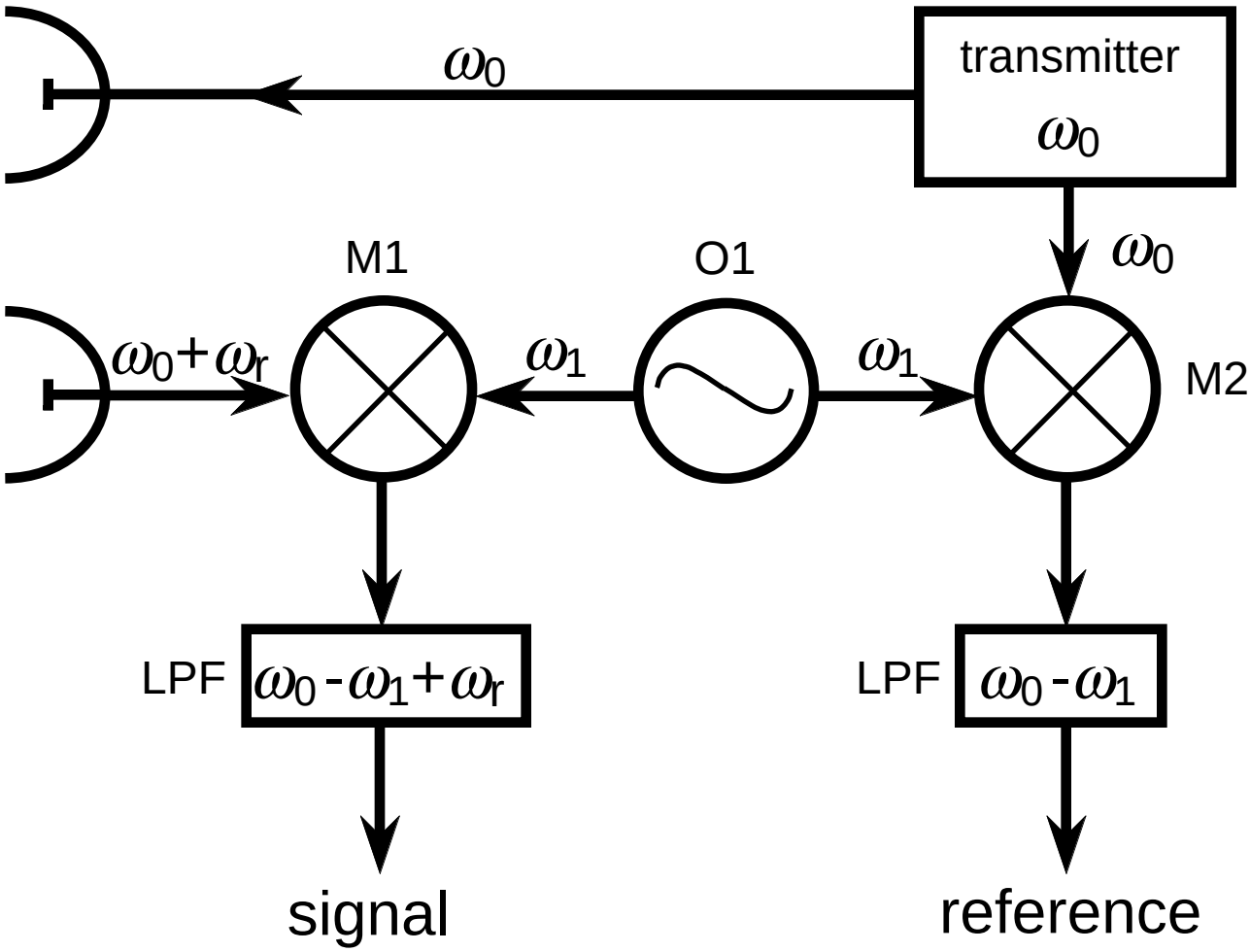
ω_0
transmitter
ω_0
ω_0
M1
O1
M2
$\omega_0+\omega_r$
ω_1
ω_1
LPF
$\omega_0-\omega_1+\omega_r$
LPF
$\omega_0-\omega_1$
signal
reference

Fig. 10

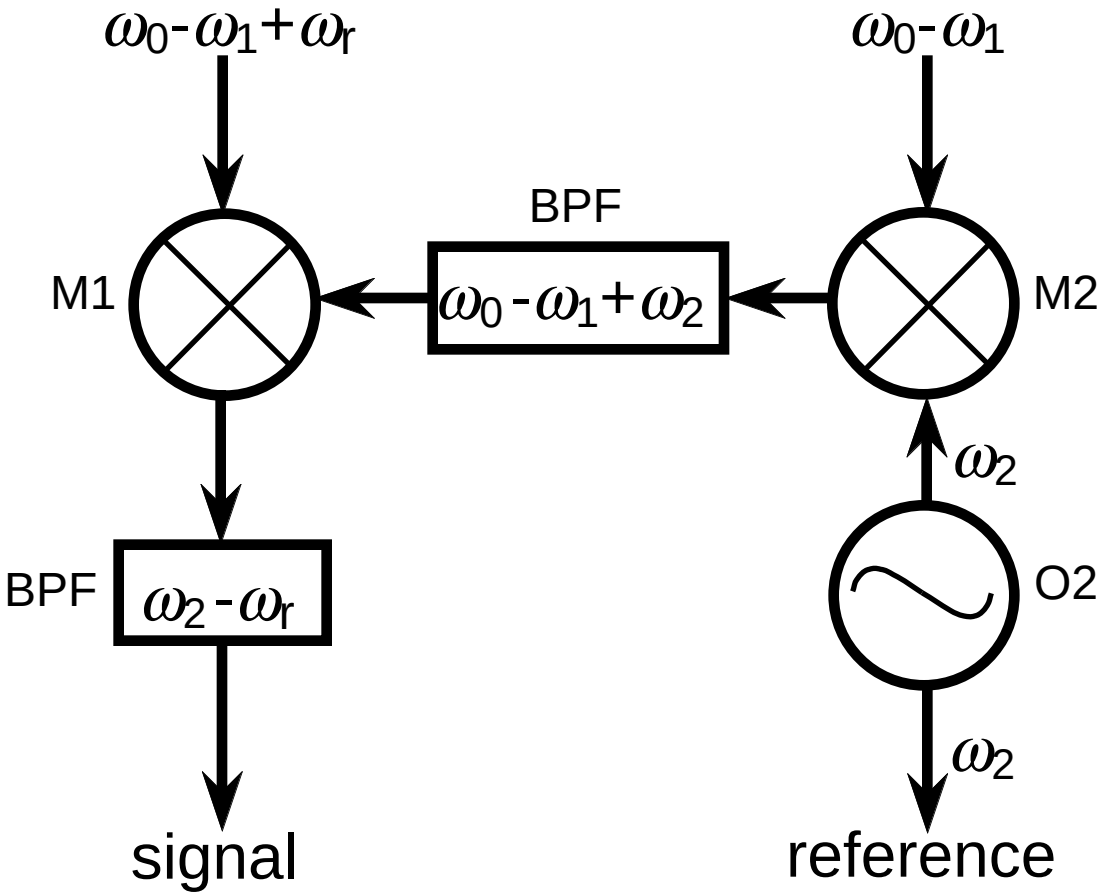
$\omega_0-\omega_1+\omega_r$
$\omega_0-\omega_1$
BPF
M1
$\omega_0-\omega_1+\omega_2$
M2
ω_2
BPF
$\omega_2-\omega_r$
O2
ω_2
signal
reference

Fig. 11

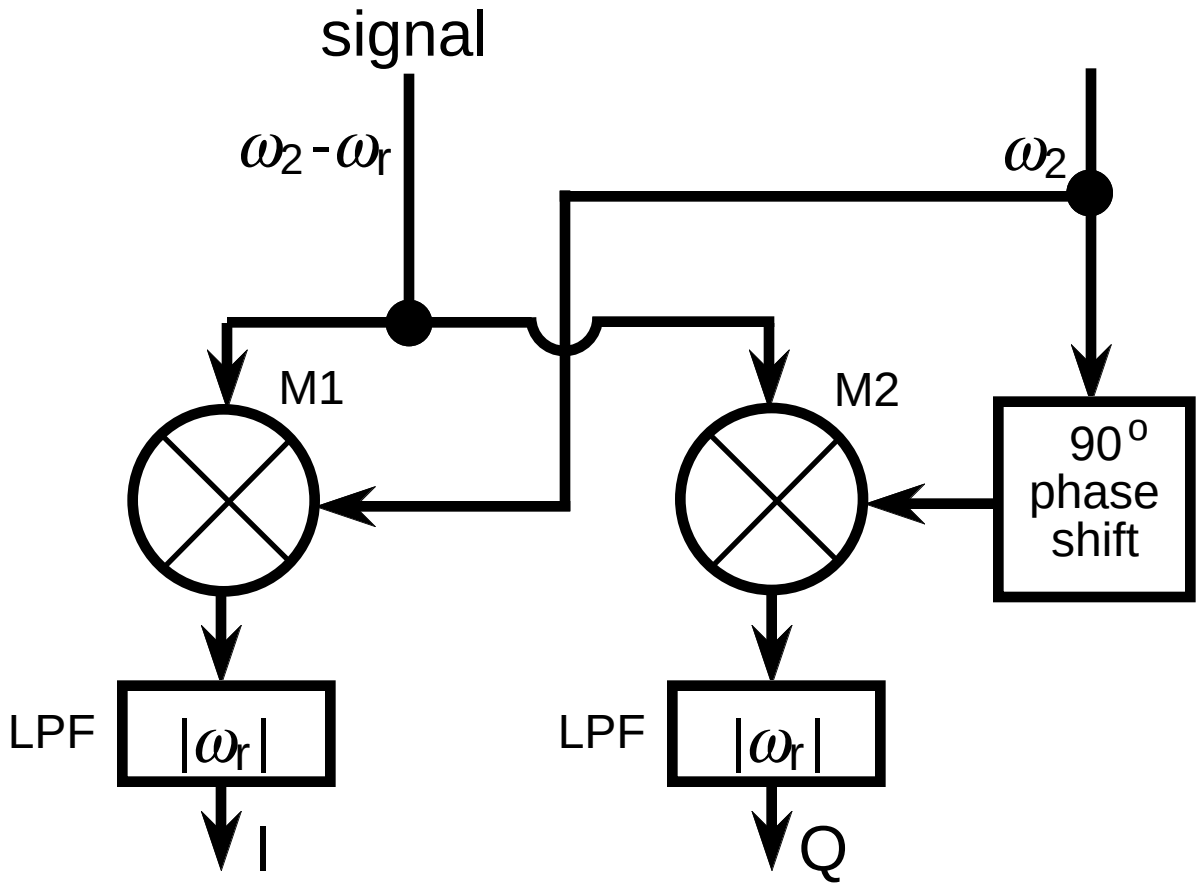
signal
$\omega_2 - \omega_r$
ω_2
M1
M2
90 o
phase
shift
LPF
$|\omega_r|$
LPF
$|\omega_r|$
I
Q

Fig. 12

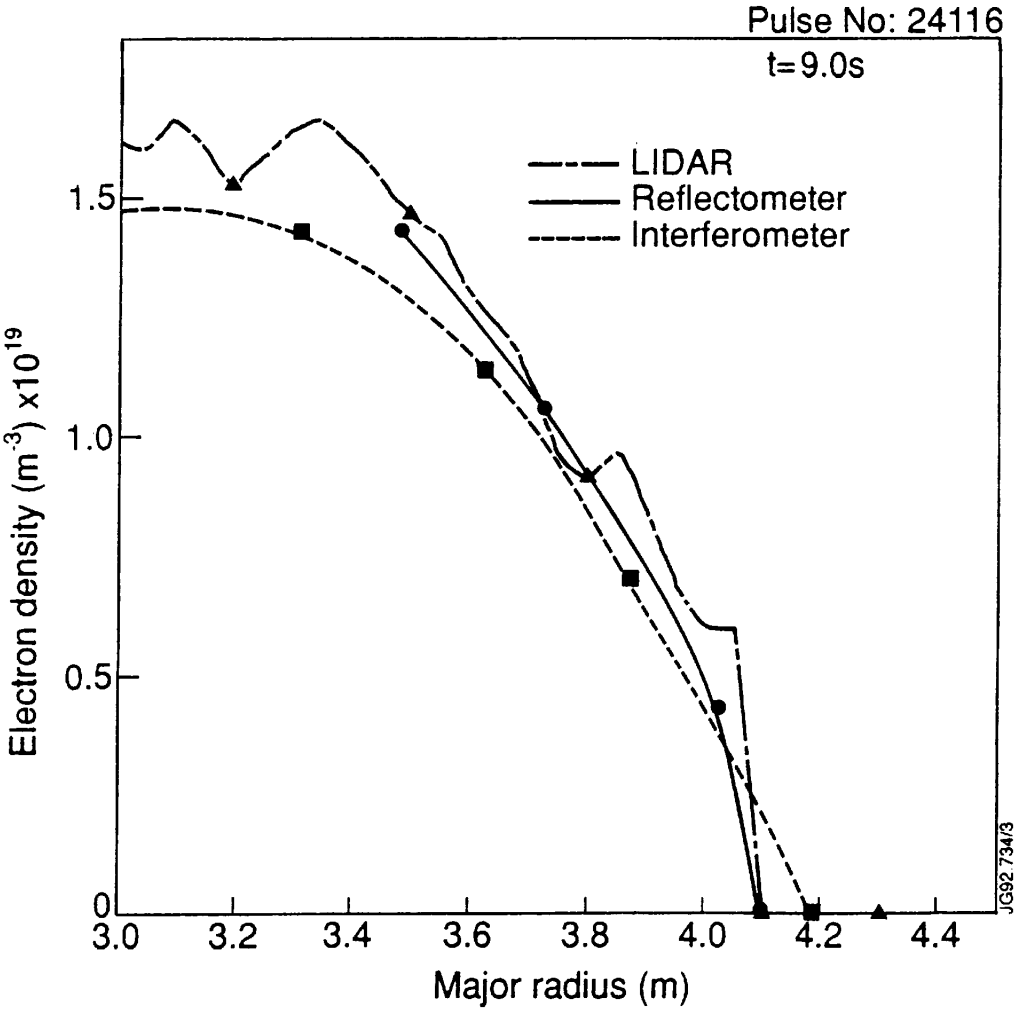
Pulse No: 24116
t=9.0s
LIDAR
Reflectometer
Interferometer
Electron density (m^{-3}) x10^{19}
1.5
1.0
0.5
0
3.0
3.2
3.4
3.6
3.8
4.0
4.2
4.4
Major radius (m)
JG92.734/3

Fig. 13

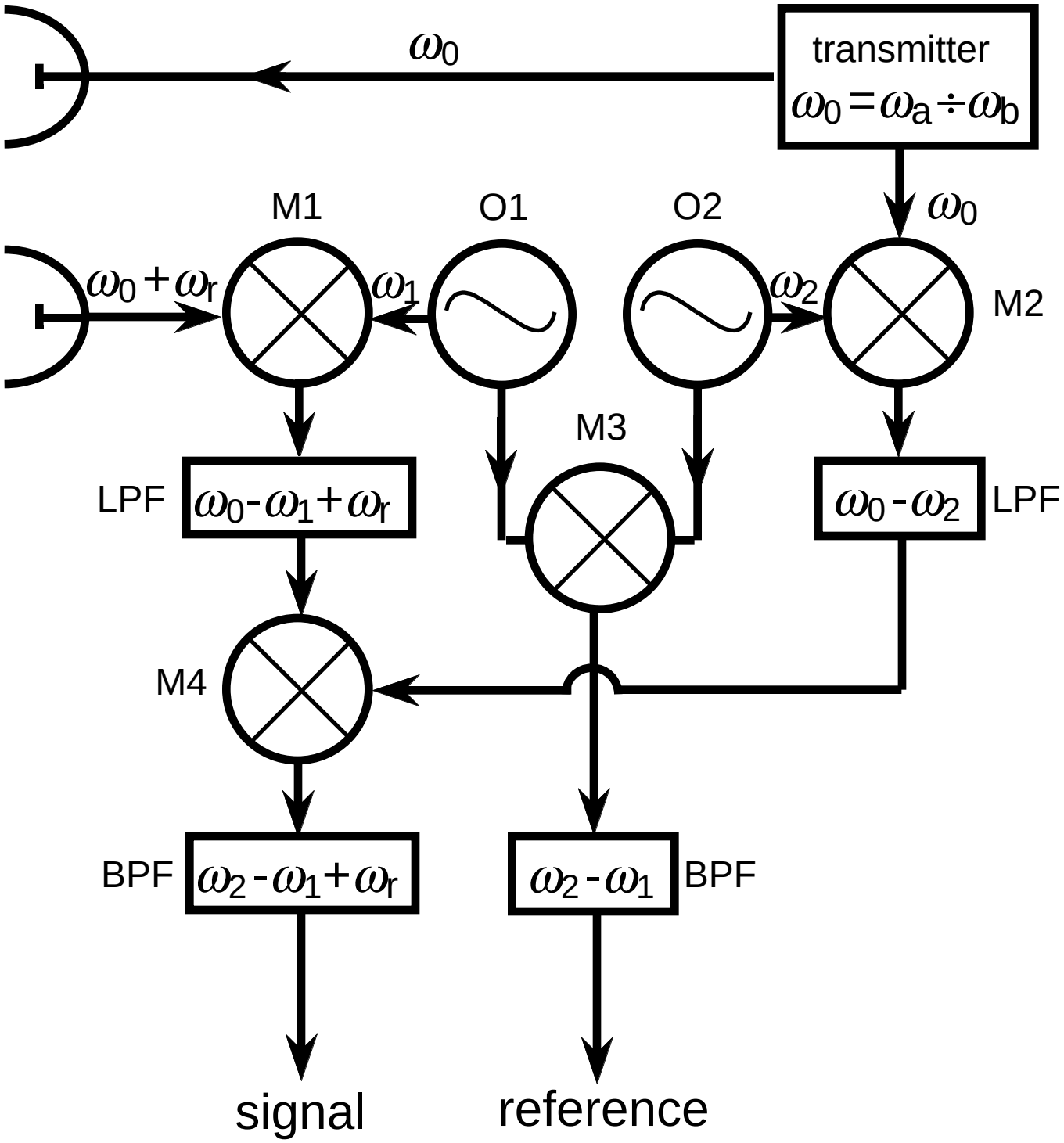
ω_0
transmitter
$\omega_0 = \omega_a \div \omega_b$
M1
O1
O2
ω_0
$\omega_0 + \omega_r$
ω_1
ω_2
M2
M3
LPF
$\omega_0 - \omega_1 + \omega_r$
$\omega_0 - \omega_2$
LPF
M4
BPF
$\omega_2 - \omega_1 + \omega_r$
$\omega_2 - \omega_1$
BPF
signal
reference

Fig. 14

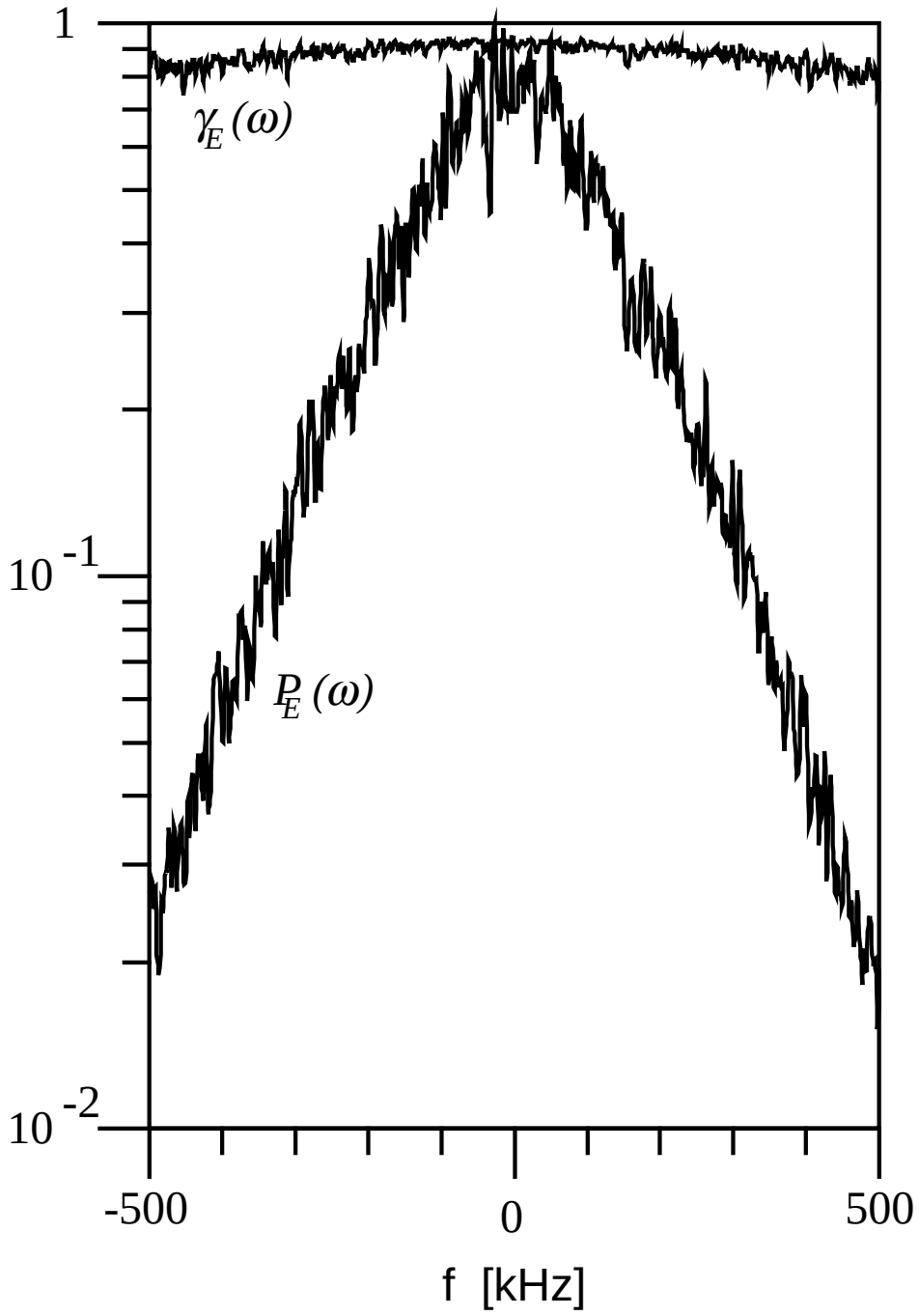

Fig. 15

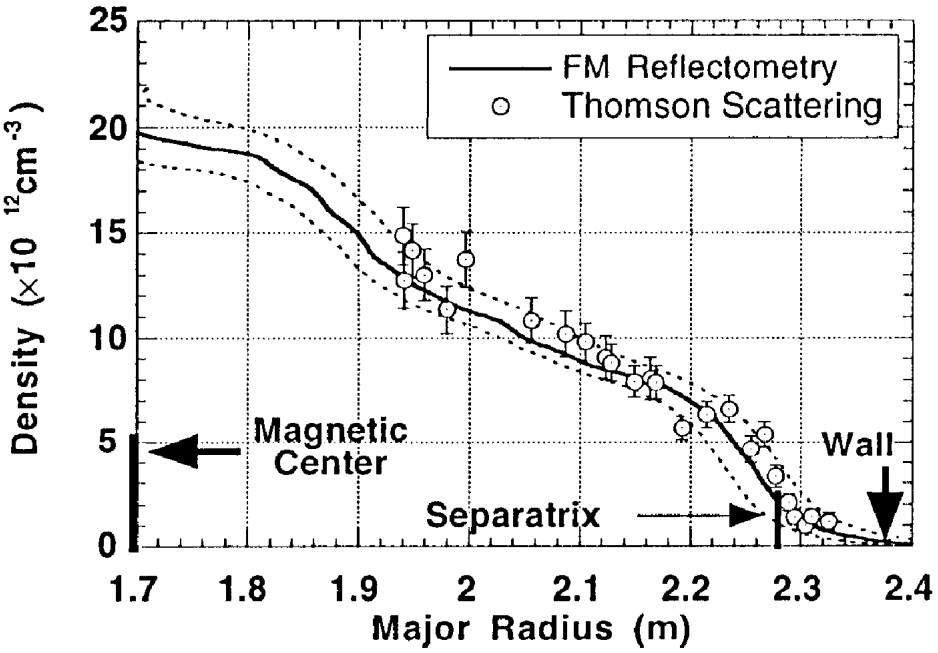
25
20
15
10
5
0
Density (×10 ^{12}cm^{-3})
FM Reflectometry
Thomson Scattering
Magnetic Center
Separatrix
Wall
1.7
1.8
1.9
2
2.1
2.2
2.3
2.4
Major Radius (m)

Fig. 16

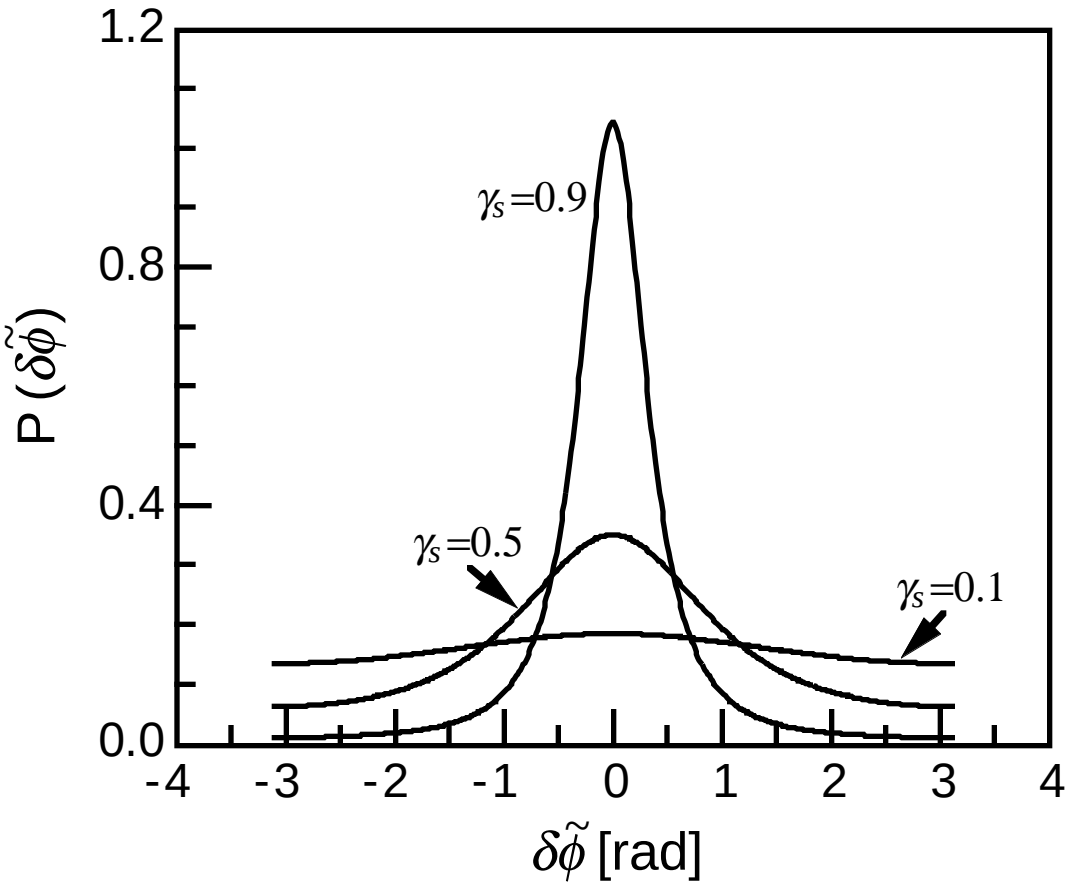
1.2
0.8
0.4
0.0
P ($\delta\tilde{\phi}$)
γ_s=0.9
γ_s=0.5
γ_s=0.1
-4
-3
-2
-1
0
1
2
3
4
$\delta\tilde{\phi}$ [rad]

Fig. 17

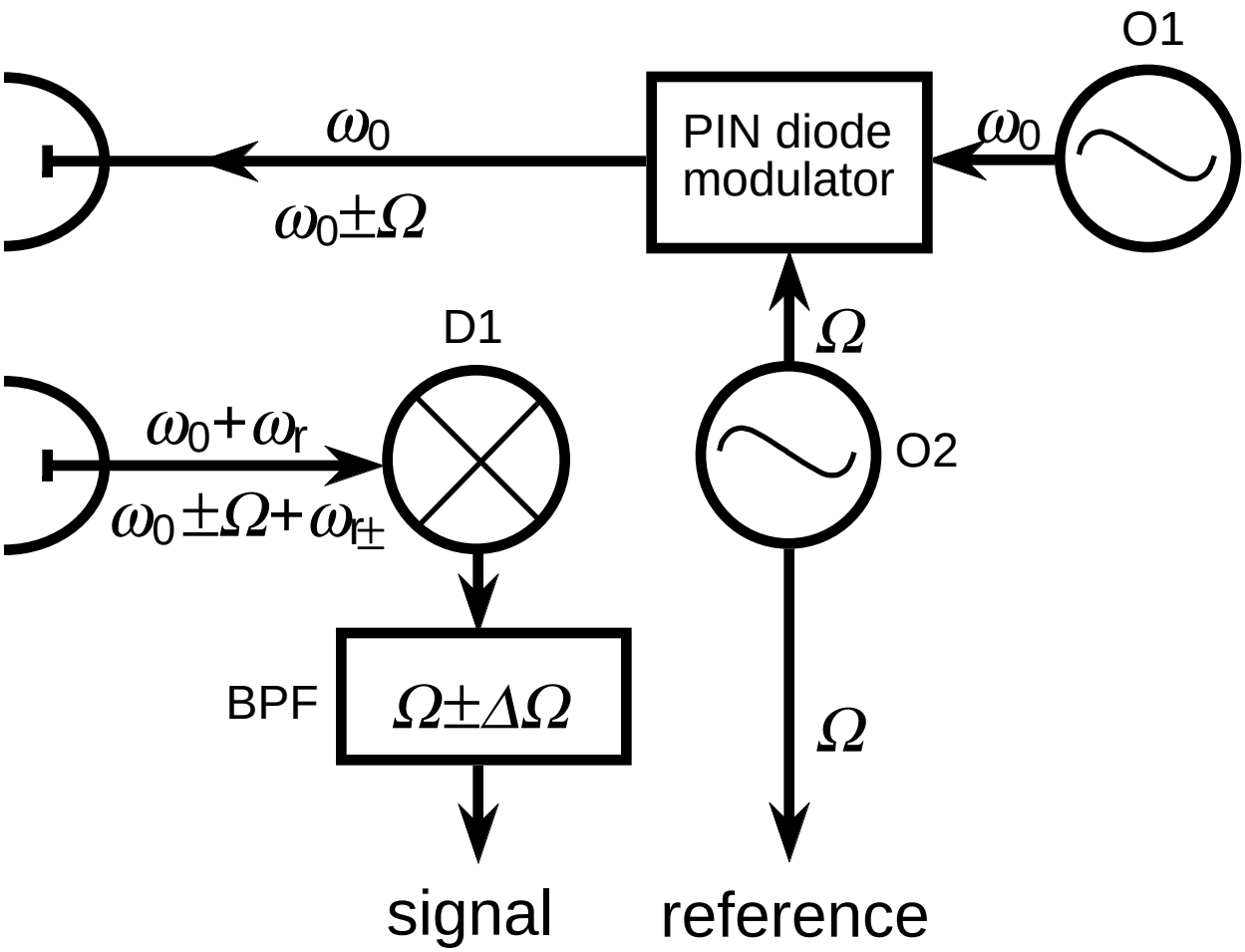
O1
PIN diode
modulator
ω_0
ω_0
$\omega_0 \pm \Omega$
D1
Ω
$\omega_0 + \omega_r$
$\omega_0 \pm \Omega + \omega_{r\pm}$
O2
BPF
$\Omega \pm \Delta\Omega$
Ω
signal
reference

Fig. 18

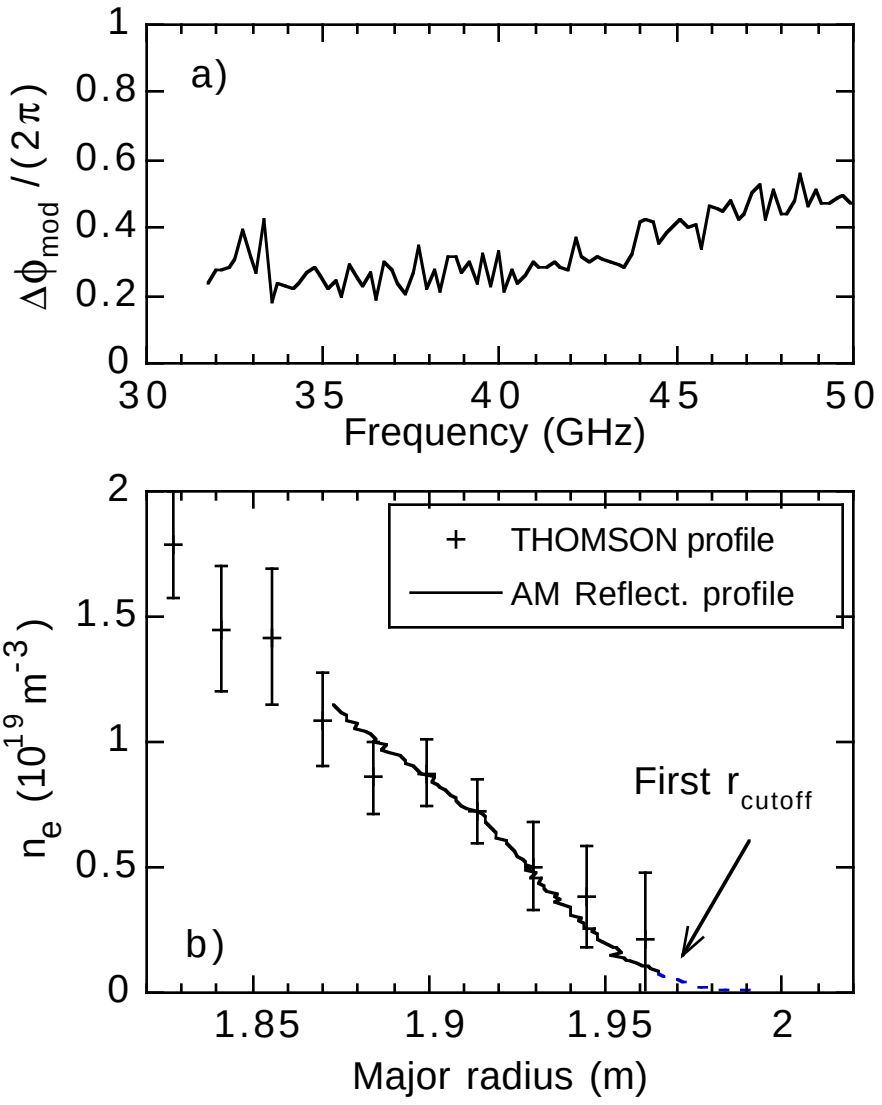
a)
$\Delta\phi_{mod}/(2\pi)$
Frequency (GHz)
b)
THOMSON profile
AM Reflect. profile
First r_{cutoff}
n_e (10^{19} m^{-3})
Major radius (m)

Fig. 19

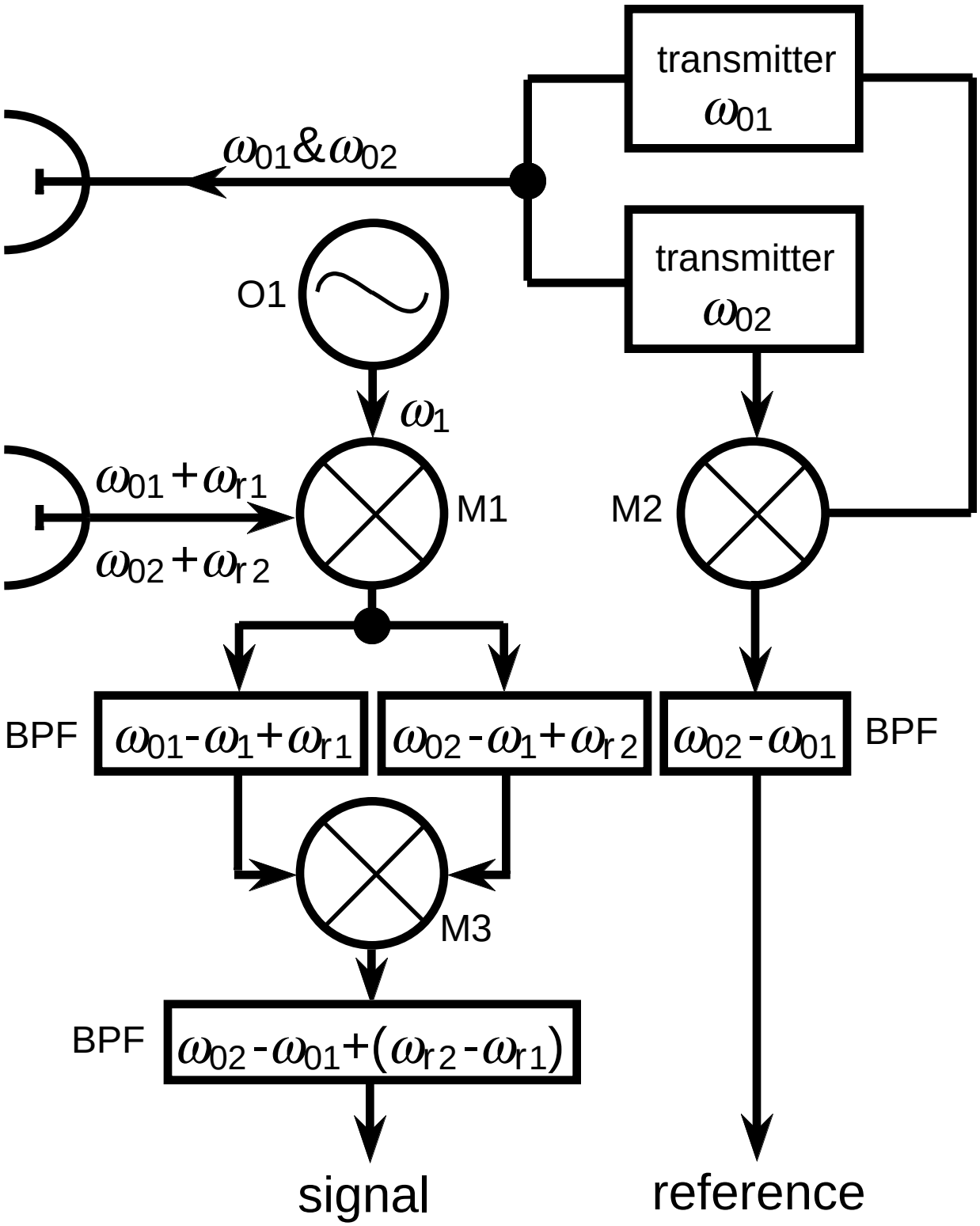
transmitter
ω_{01}
$\omega_{01}\&\omega_{02}$
transmitter
ω_{02}
O1
ω_1
$\omega_{01}+\omega_{r1}$
$\omega_{02}+\omega_{r2}$
M1
M2
BPF
$\omega_{01}-\omega_1+\omega_{r1}$
$\omega_{02}-\omega_1+\omega_{r2}$
$\omega_{02}-\omega_{01}$
BPF
M3
BPF
$\omega_{02}-\omega_{01}+(\omega_{r2}-\omega_{r1})$
signal
reference

Fig. 20

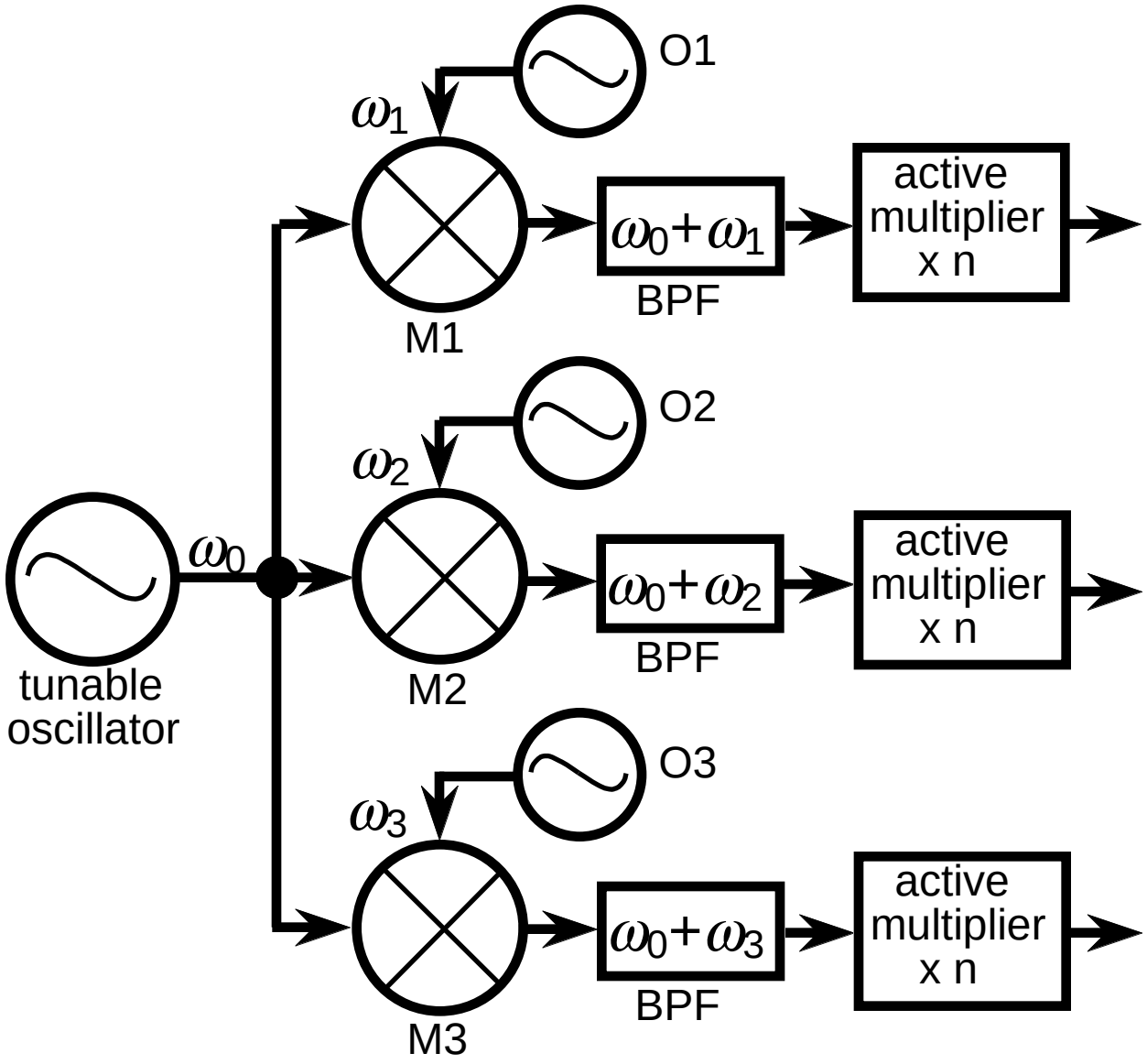
O1
ω_1
$\omega_0+\omega_1$
BPF
active
multiplier
x n
M1
O2
ω_2
ω_0
$\omega_0+\omega_2$
BPF
active
multiplier
x n
tunable
oscillator
M2
O3
ω_3
$\omega_0+\omega_3$
BPF
active
multiplier
x n
M3

Fig. 21

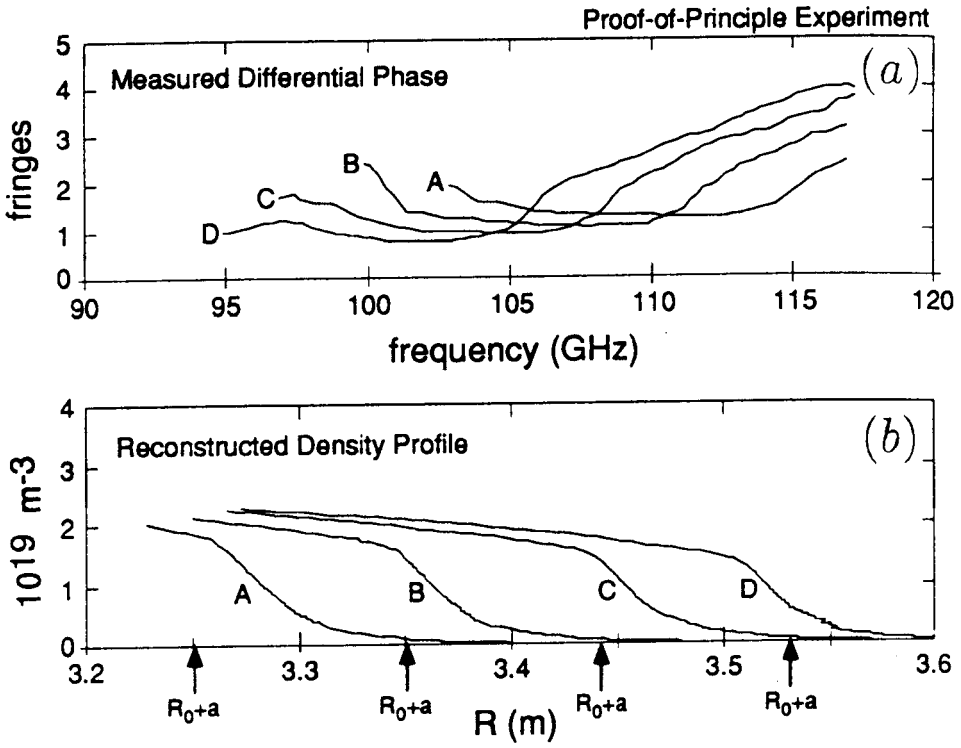
Proof-of-Principle Experiment
Measured Differential Phase
(a)
fringes
5
4
3
2
1
0
A
B
C
D
90
95
100
105
110
115
120
frequency (GHz)
Reconstructed Density Profile
(b)
1019 m-3
4
3
2
1
0
A
B
C
D
3.2
3.3
3.4
3.5
3.6
R0+a
R0+a
R0+a
R0+a
R (m)

Fig. 22

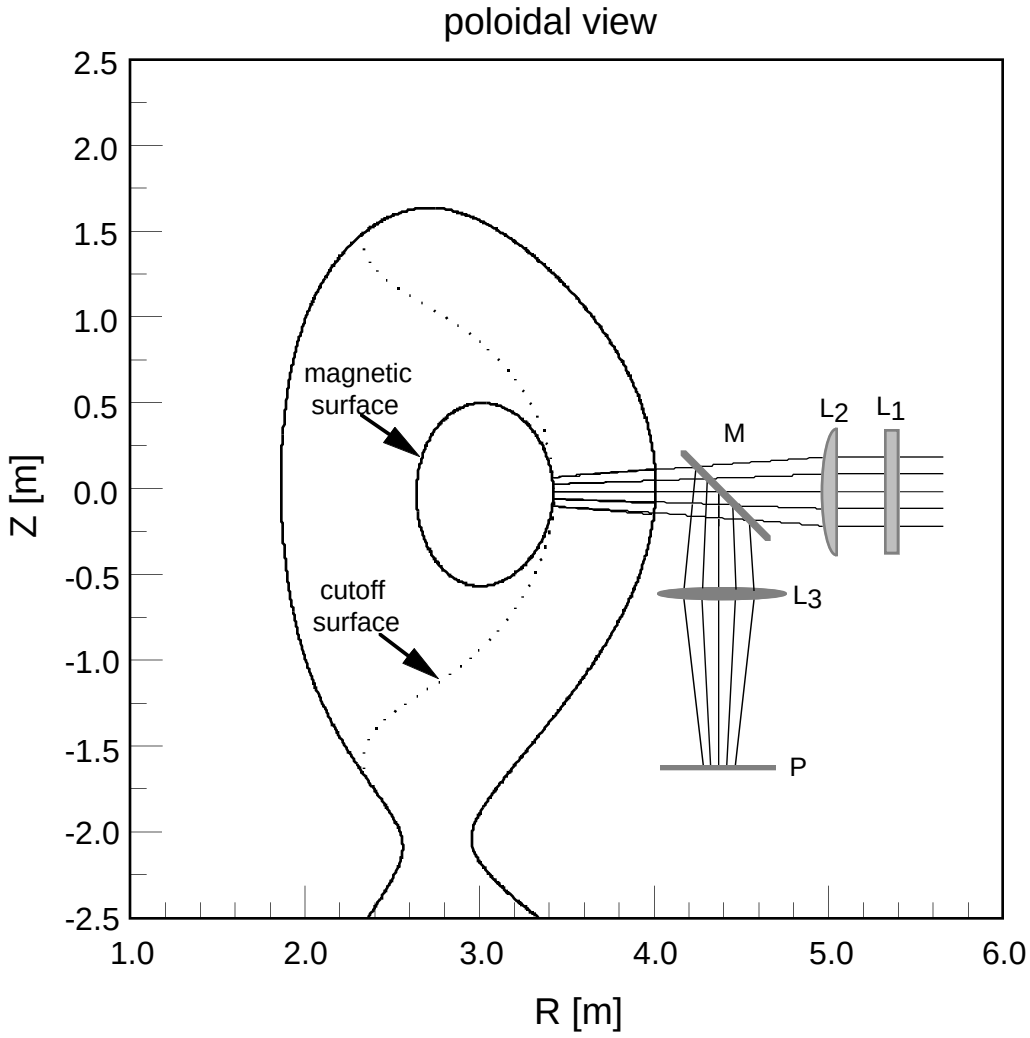
poloidal view
2.5
2.0
1.5
1.0
0.5
0.0
-0.5
-1.0
-1.5
-2.0
-2.5
Z [m]
1.0
2.0
3.0
4.0
5.0
6.0
R [m]
magnetic surface
cutoff surface
M
L2
L1
L3
P

Fig. 23